

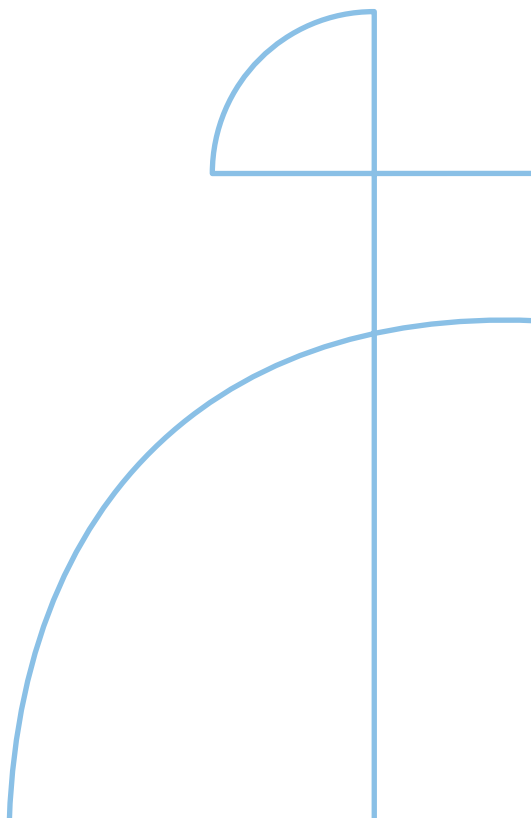


Doctoral Thesis in Fibre and Polymer Science

# Lignin-Rich Microfibrillated Cellulose Films: From Production to Application

HUISI LI

KTH ROYAL INSTITUTE OF TECHNOLOGY



# Lignin-Rich Microfibrillated Cellulose Films: From Production to Application

HUISI LI

Academic Dissertation which, with due permission of the KTH Royal Institute of Technology, is submitted for public defence for the Degree of Doctor of Philosophy on Thursday the 12th December 2024, at 10.00 a.m. in F3, Lindstedtsvägen 26, Stockholm.

Doctoral Thesis in Fibre and Polymer Science  
KTH Royal Institute of Technology  
Stockholm, Sweden 2024

© Huisi Li

ISBN 978-91-8106-123-9  
TRITA-CBH-FOU-2024:56

Printed by: Universitetservice US-AB, Sweden 2024

*To my family*

学无止境



# Abstract

Lignocellulosic biomass, particularly wood-derived cellulose, offers an abundant and renewable resource for producing advanced bio-based materials. This thesis explores the development and application of lignin-rich microfibrillated cellulose (LMFC) films produced from high-kappa number kraft pulp, highlighting their potential as sustainable alternatives to petrochemical-based materials. The research focuses on understanding the influence of residual lignin and raw fiber characteristics on the properties of LMFC films. The effects of drying conditions on the physicochemical and mechanical properties of these films were also investigated.

The study demonstrates that residual lignin enhances the thermal stability and hydrophobicity of the films while also improving their mechanical properties under optimized processing conditions. Furthermore, hardwood and softwood pulps exhibit distinct fibrillation behaviors, with softwood-derived LMFC films showing superior tensile strength due to the formation of more fiber joints within the fiber networks. The exceptional mechanical performance of LMFC films, comparable to chemically modified cellulose nanofibers, demonstrates their potential for industrial applications. These lignin-rich films show promise in high-value fields such as battery, organic dye adsorption, and proton exchange application. Notably, LMFC films are ideal candidates as separators in aqueous zinc-ion batteries, where their enhanced wet tensile strength, superior electrolyte uptake, and good ionic conductivity enable stable cycling performance. Additionally, the films' enhanced affinity for cationic organic dyes positions them as effective and eco-friendly adsorbents for water treatment. The findings of this thesis contribute to the sustainable development of bio-based cellulose materials by optimizing lignocellulosic resources for a wide range of applications.

## **Keywords**

Lignin-rich cellulose, microfibrillated cellulose, cellulose film, drying, bio-based materials, separator, dye adsorption, proton exchange.

# Sammanfattning

Biomassa från lignocellulosa, särskilt cellulosa från trä, utgör en rikligt förekommande och förnybar resurs för produktion av avancerade biobaserade material. Denna avhandling undersöker utvecklingen och tillämpningen av ligninrik mikrofibrillerad cellulosa (LMFC)-filmer, framställda av hög-kappa sulfatmassa, och belyser dess potential som hållbart alternativ till petrokemiskt baserade material. Forskningen fokuserar på att förstå hur restlignin och råfiberkaraktäristika påverkar egenskaperna hos LMFC-filmer. Effekterna av torkningsförhållanden på de fysikalisk-kemiska och mekaniska egenskaperna hos dessa filmer undersöktes också.

Studien visar att restlignin ökar den termiska stabiliteten och hydrofobiciteten hos filmerna samt förbättrar deras mekaniska egenskaper under optimerade bearbetningsförhållanden. Vidare uppvisar lövträ- och barrträmassor olika fibrilleringsbeteenden, där LMFC-filmer framställda från barrträ visar överlägsen draghållfasthet på grund av bildningen av fler fiberförbindelser inom fibernätverket. Den exceptionella mekaniska prestandan hos LMFC-filmer, jämförbar med kemiskt modifierade cellulosanofibrer, visar deras potential för industriella tillämpningar. Dessa ligninrika filmer har lovande användningsområden inom högvärdesfält som batterier, organisk färgadsorption och protonutbyte tillämpningar. Särskilt LMFC-filmer är idealiska kandidater som separatorer i vattenbaserade zink-jonbatterier, där deras förbättrade våtstryka, överlägsna elektrolytupptag och goda jonledningsförmåga möjliggör stabil cyklingsprestanda. Dessutom ger filmernas ökade affinitet för katjoniska organiska färgämnen dem till effektiva och miljövänliga adsorbenter för vattenrening. Resultaten i denna avhandling bidrar till hållbar utveckling av biobaserade cellulosa material genom optimering av lignocellulosaresurser för ett brett spektrum av tillämpningar.

## Nyckelord

Ligninrik cellulosa, mikrofibrillerad cellulosa, cellulosa film, torkning, biobaserade material, separator, färgadsorption, protonutbyte.

# List of publications

## Paper I

### **Enhancing the strength and flexibility of microfibrillated cellulose films from lignin-rich kraft pulp**

Huisi Li, Artem Kulachenko, Aji P. Mathew, Raquel Bohn Stoltz, Olena Sevastyanova (2023). ACS Sustainable Chemistry & Engineering, 11(47), 16793-16805.

## Paper II

### **A comparative study of lignin-containing microfibrillated cellulose fibers produced from softwood and hardwood pulps**

Huisi Li, Bin Chen, Artem Kulachenko, Vilhelmine Jurkjane, Aji P. Mathew, Olena Sevastyanova (2024). *Cellulose*, 31(2), 907-926.

## Paper III

### **Eco-friendly and strong lignin-containing microfibrillated cellulose films for high-performance separators of aqueous zinc batteries**

Huisi Li, Sadegh Askari, Artem Kulachenko, Monica Ek, Olena Sevastyanova (2024). (Submitted after review to International Journal of Biological Macromolecules)

## Paper IV

### **Lignocellulose-derived membranes for efficient separation and removal of synthetic dyes from water**

Oleg Tkachenko, Huisi Li, Galina Dobeleva, Olena Sevastyanova, Tetyana M. Budnyak (2024). (Submitted Manuscript)

## Paper V

### **Lignin-rich microfibrillated cellulose: A Sustainable alternative for proton exchange membranes for energy applications**

Huisi Li, Roman Selyanchyn, Shigenori Fujikawa, Artem Kulachenko, Olena Sevastyanova (2024). (Manuscript)

## Contributions to the papers

- Paper I      The first author, the major part of the conceptualization, planned and performed all experiments, analyzed all data, and wrote the manuscript.
- Paper II     The first author, the major part of the conceptualization, planned and performed most of the experiments, analyzed all corresponding data, and wrote the manuscript.
- Paper III    The first author, the major part of the conceptualization, planned and performed most of the experiments, analyzed all data, and wrote the manuscript.
- Paper IV    Co-author, planned and performed part of the experiments, analyzed corresponding data, and wrote part of the manuscript (corresponding parts in the introduction, experimental, and results and discussion).
- Paper V     The first author, planned and performed part of the experiments, analyzed corresponding data, and wrote the manuscript.

# Scientific papers not included in the thesis

## **Surface chemistry and bioactivity of colloidal particles from industrial kraft lignins**

Oihana Gordobil, [Huisi Li](#), Ana Ayerdi Izquierdo, Ainhoa Egizabal, Olena Sevastyanova, Anna Sandak. (2022) International Journal of Biological Macromolecules, 220, 1444-1453.

## **Exploring the physicochemical and rheological properties of sustainable asphalt binders modified with lignin and high-viscosity additive**

Wangjie Wu, [Huisi Li](#), Olena Sevastyanova, Nicole Kringos, Maria Chiara Cavalli. (2024) Construction and Building Materials, 450, 138621.

# List of abbreviations

MFC	Microfibrillated Cellulose
LMFC	Lignin-Rich Microfibrillated Cellulose
TOCNF	TEMPO-Oxidized Cellulose Nanofibers
BSKP	Bleached Softwood Kraft Pulp
LSKP	Lignin-rich Softwood Kraft Pulp
LHKP	Lignin-rich Hardwood Kraft Pulp
SW	Softwood
HW	Hardwood
SGW	Simulated Groundwater
ARW	Actual River Water
SEM	Scanning Electron Microscopy
EIS	Electrochemical Impedance Spectroscopy
DIC	Digital Image Correlation
FTIR	Fourier Transform Infrared Spectroscopy
TGA	Thermogravimetric Analysis
SS	Stainless Steel
MB	Methylene Blue
CV	Crystal Violet
PEM	Proton Exchange Membrane
FC	Fuel Cell
RH	Relative Humidity
AZIB	Aqueous Zinc-Ion Battery
KOH	Potassium Hydroxide
KF	Potassium Fluoride
NaOH	Sodium Hydroxide

# CONTENTS

1	Introduction .....	1
1.1	Wood structures and compositions .....	1
1.2	Structures and functions of lignin in wood.....	3
1.3	Preparation of lignin-rich nano/micro-cellulose .....	4
1.3.1	Mechanical treatments.....	5
1.3.2	Chemical treatments .....	6
1.3.3	Other treatments .....	6
1.4	Overview of the production of nano/micro-cellulose films.....	7
1.4.1	Casting method .....	7
1.4.2	Coating method .....	8
1.4.3	Filtration method .....	8
1.5	Thesis aim and objectives .....	9
1.6	Sustainability .....	11
2	Materials and methods .....	13
2.1	Materials and chemicals.....	13
2.2	Experimental methods.....	13
2.3	Characterization techniques .....	14
3	Results and discussion.....	21
3.1	Characterization of raw pulps .....	22
3.2	Effect of residual lignin.....	23
3.3	Influence of raw fibers .....	27
3.4	Effect of drying conditions .....	33
3.5	Applications of lignin-rich nano/micro-cellulose films.....	36
3.6	Recyclability .....	47
4	Summary of the thesis.....	51
5	Conclusions .....	55
6	Future outlook .....	57
7	Acknowledgments .....	59
8	References .....	61



# 1 Introduction

The excessive use of fossil fuels has led to numerous environmental and health problems. Burning fossil fuels releases large quantities of carbon dioxide and other greenhouse gases into the atmosphere, contributing significantly to global warming and climate change<sup>1,2</sup>. This results in more frequent and severe weather events, rising sea levels, and disruptions to ecosystems. To address these concerns and the diminishing supply of petrochemical resources, converting abundant lignocellulosic biomass into green energy, chemicals, and materials has become a highly attractive area of research<sup>3,4</sup>. Lignocellulosic biomass, which makes up about 90% of the Earth's fixed energy content, offers a substantial resource for biomass conversion and utilization to replace plastic-based products<sup>5,6</sup>. This shift can help reduce environmental pollution and lower the carbon footprint.

## 1.1 Wood structures and compositions

Wood is a complex lignocellulosic material with a hierarchical structure, ranging from the macroscale of wood stem to the nanoscale in cell walls, as depicted in Figure 1. The wood cell wall is composed of three primary biopolymers: cellulose, hemicellulose, and lignin, along with various extractives. These components are intricately organized to form a composite material that endows wood with its unique mechanical properties and durability. Specifically, cellulose, accounting for 40-50 wt% of cell walls, in the form of microfibril bundles are embedded in the matrix of hemicellulose (10-30 wt%) and lignin (roughly 20-30 wt% of cell wall structures)<sup>7,8</sup>. Their composition varies among different wood species, individuals, and among different parts from the same individual<sup>5,8</sup>.

Cellulose is a linear macromolecule, which is composed of long chains of glucose units linked by  $\beta$ -1,4-glycosidic bonds. These cellulose molecules align in a parallel pattern and are assembled into long elementary fibrils *via* hydrogen bonds<sup>7,9</sup>. Hemicellulose is a branched polymer with a lower degree of polymerization (150-200), as shown in Figure 1b. It is a group of heterogeneous polysaccharides comprising various sugar monomers, including xylose, mannose, glucose, galactose, arabinose, and other monosaccharides. Lignin, a complex and irregular polymer of phenylpropane units, contributes to the rigidity and resistance to decay of wood. In addition to these primary components, wood contains inorganic components, and low-molecular-weight organic compounds such as tannins, suberin, and resins<sup>8</sup>.

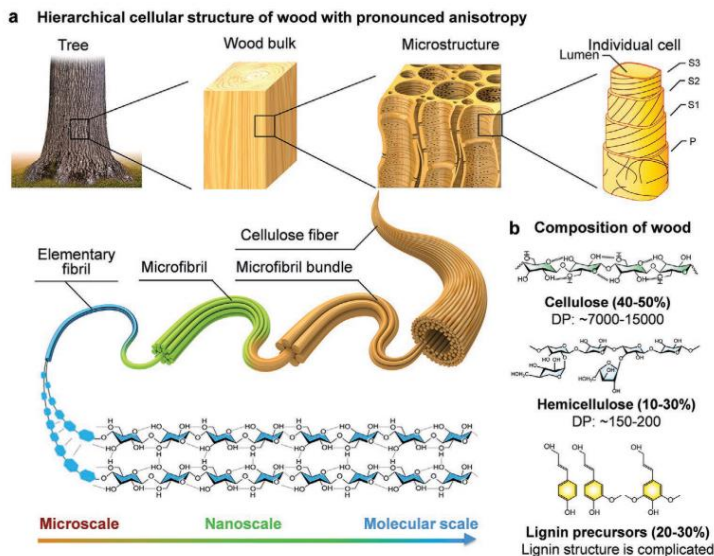


**Figure 1.** a) Schematic illustration of hierarchical wood structures at multiple scales, b) three main components of wood (Figure adapted with permission)<sup>7</sup>.

Wood cell walls are composed of several layers at the ultrastructural level, namely, middle lamella (M), primary wall (P), and secondary cell wall (S1, S2, and S3). The highly lignified middle lamella functions as a binder between neighboring cells. The primary cell wall is a thin layer containing cellulose, hemicelluloses, pectin, and protein, which are completely embedded in lignin<sup>10,11</sup>. The secondary cell wall consists of three layers with cellulose microfibrils assembled at different angles to the axial fiber direction in each layer, with the middle layer (S2) forming the main component of the cell walls.

The low microfibrillar angle of the fibrillar network with respect to the fiber axis significantly contributes to the mechanical strength and stiffness<sup>4,12</sup>.

## **1.2 Structures and functions of lignin in wood**

Lignin, a complex polymer present in the cell walls of wood and other vascular plants, plays fundamental roles in their structural integrity and functional properties. It is primarily composed of three monolignols: p-coumaryl alcohol, coniferyl alcohol, and sinapyl alcohol. These monolignols are aromatic alcohols with distinct structures contributing to the diversity of lignin units found in plant tissues. p-Coumaryl alcohol shows no methoxy group on its structures, giving rise to p-hydroxyphenyl (H) units in lignin. Coniferyl alcohol, characterized by a single methoxy group (-OCH<sub>3</sub>) on the aromatic ring, forms guaiacyl (G) units. Sinapyl alcohol, with two methoxy groups, contributes to syringyl (S) units<sup>13,14</sup>. These monolignols undergo enzymatic oxidative coupling reactions catalyzed by peroxidases and laccases, leading to the polymerization through various chemical linkages to form a three-dimensional network that provides strength and rigidity to the plant cell walls<sup>15,16</sup>.

The monolignol composition of lignin varies significantly depending on the plant species. In softwoods, lignin primarily comprises G units formed by coniferyl alcohol. In contrast, hardwood lignins consist mainly of S and G units formed from sinapyl and coniferyl alcohol. These variations in monolignol composition result in distinct structural properties of lignin between softwoods and hardwoods<sup>16,17</sup>. In wood, lignin is a vital component of plant cell walls, particularly in the secondary and middle lamella. It serves several essential functions for wood structures. Firstly, it provides structural support by filling the spaces between cellulose microfibrils, hemicellulose, and other components of the cell wall matrix. This binding function of lignin reinforces the cell wall structures, enhancing its mechanical strength and stiffness. Secondly, lignin's hydrophobic nature plays a crucial role in regulating water transport within the plant. Furthermore, lignin acts as a barrier against pathogens and pests, thereby enhancing the resistance of wood to decay and degradation over time. Additionally, lignin exhibits good antioxidant properties and UV light absorption, which protect the underlying cellulose and hemicellulose from environmental stresses<sup>16,18,19</sup>. However, in the conventional pulp and paper industry, removing lignin is essential to produce fully bleached pulp with a high content of carbohydrates and a higher level of brightness and whiteness. Industrial delignification of lignocellulosic biomass is typically achieved through

pulping, oxygen delignification, and bleaching stages to eliminate lignin. However, the use of harsh chemicals in the delignification process to remove residual lignin not only poses significant environmental concerns but also increases the overall cost of production, making the process less sustainable and economically efficient. Furthermore, the function of lignin in wood indicates the potential to utilize lignin in preparing functional materials.

### **1.3 Preparation of lignin-rich nano/micro-cellulose**

Nanocelluloses produced from wood-based fibers have attracted great interest owing to their superior mechanical properties, abundance, as well as their renewable and biodegradable characteristics<sup>4,20</sup>. Generally, nanocelluloses can be categorized into two main types: cellulose nanocrystals (CNC) and cellulose nanofibrils (CNF), CNF is also known as microfibrillated cellulose, nanofibrillated cellulose (NFC) or cellulose nanofibers<sup>4</sup>. both types are excellent alternatives to petroleum-based polymers in the fields of papermaking, composites, and packaging, among others<sup>21–23</sup>.

Recently, the focus has shifted towards lignin-containing nanocellulose owing to the lower cost and higher yield of unbleached pulp and new functionalities provided by lignin, including higher hydrophobicity, improved compatibility with non-polar matrices, increased thermal stability<sup>5,6</sup>. The higher resource efficiency from using lignin-containing pulps, in combination with the unique characteristics provided by remaining lignin, makes producing lignin-containing nanocelluloses very interesting for technical usage in UV-protection, adsorption, and energy storage applications, as well as a reinforcement component in nanocomposites<sup>24–28</sup>. Notably, the use of high lignin content raw materials reduces the need for extensive pulp delignification process, simplifying the processing and resulting in lower-cost materials.

Generally, the preparation of lignin-containing cellulose materials follows a similar sequence to that of conventional pure nanocelluloses. The key distinguishing factor lies in the extent of delignification of the raw fibers used. So far, different techniques have been used to prepare lignocellulose nano/micromaterials. These techniques can be categorized into mechanical treatments (refining, grinding, high-pressure homogenization, and microfluidization)<sup>4</sup>, chemical treatments (inorganic acid hydrolysis<sup>29</sup>, carboxymethylation<sup>30</sup>, TEMPO-mediated oxidation<sup>22,31</sup> and enzymatic hydrolysis)<sup>32</sup>. Innovative preparation methods are being introduced in alignment with the principles of green and sustainable chemistry. These include

organic acid hydrolysis (using acids such as formic acid, maleic acid, and oxalic acid) and deep eutectic solvent (DES) treatments for lignocellulose nano/micromaterials production<sup>5</sup>.

### 1.3.1 Mechanical treatments

The defibrillation of cellulose fibers into CNF requires intensive mechanical treatments. These methods primarily rely on physical forces to break down cellulose fibers into nano or micro-scale structures while not significantly affecting the lignin content. The main mechanical techniques for producing lignin-containing nano/micro cellulose fibers include refining, grinding, and high-pressure homogenization, among others<sup>4</sup>.

Refining utilizes mechanical refining equipment such as disk refiners<sup>33</sup>, PFI mills<sup>34</sup>, and Valley beaters<sup>35</sup> to swell and disintegrate the fiber's cell wall in an aqueous medium, which is commonly used in the paper and pulp industry. Refining can enhance fiber's specific surface to make it more accessible for further biological or chemical treatment. However, refining also decreases the fiber length *via* cutting and increases the fine content<sup>4</sup>. Grinding involves the use of mechanical shear forces to reduce the size of cellulose fibers, breaking down the fibers into smaller, nanoscale, or microscale particles<sup>35</sup>. During the grinding process, the cellulose slurry is passed between static and rotating grinding stones, and the distance between these disks can be adjusted. High-pressure homogenization utilizes intense mechanical forces generated by high-pressure fluid jets to disintegrate cellulose fibers into nano-sized particles. The cellulose slurry is forced through a narrow gap at high pressures, breaking down fibers<sup>36</sup>. Erfan et al. prepared lignin-containing cellulose fibers with different lignin content by controlling the kraft cooking time and then subjected them to fibrillation using a PFI refiner and a high-pressure microfluidizer<sup>28</sup>. The produced lignin-containing microfibrillated cellulose fibers exhibited a lateral dimension of 2.5-0.8  $\mu\text{m}$  after fractionation, and the results also show that the nanofibril yield can be maximized due to the two competing mechanisms arising with the enhanced charge with increasing lignin content and increased cellulose fibril binding effects due to lignin. In another study, Chen et al. produced cellulose nanofibrils with high residual lignin content from polar powder using pure mechanical grinding<sup>37</sup>. Their lignin content was controlled by a reaction in an aqueous solution with glacial acetic acid and sodium chlorite, followed by mechanical fibrillation through a coarse mechanical pretreatment and then high-shear disintegration by a grinder. It was also reported that residual lignin can help prevent crystalline damage from the mechanical grinding process.

### 1.3.2 Chemical treatments

The conventional chemical methods used for preparing pure nanocelluloses have also been employed for the preparation of lignin-rich nanocelluloses, such as inorganic acid hydrolysis and TEMPO oxidation.

Inorganic acid hydrolysis, mainly using sulfuric acid or hydrochloric acid, can break down cellulose fibers into nanocrystals. Treating cellulose with concentrated acid hydrolyzes the amorphous regions of cellulose while preserving the crystalline regions<sup>38</sup>. Wang et al. produced lignin-containing cellulose nanocrystals from old newspapers using sulfuric acid hydrolysis with lignin content between 8-19wt% on the surfaces determined by XPS<sup>39</sup>. The results showed that the thermal stability and hydrophobicity of lignin-containing nanocellulose increase with the increasing lignin content but decreasing crystallinity. In another study, high-lignin-containing cellulose nanocrystals were prepared from poplar wood using a hydrothermal method followed by acid hydrolysis using sulfuric acid, and the degree of crystallinity of cellulose nanocrystals can be controlled by adjusting the temperature of the hydrothermal process<sup>40</sup>. The residual lignin was found to be distributed in the nano-form onto fibers and contributed to the high thermal stability and hydrophobicity. Ewulonu et al. reported a feasible method to produce cellulose nanofibers containing about 92% of the original lignin content of raw fibers and diameters between 15 and 26nm by using 1–3% sulfuric acid in combination with ball milling and ultrasonication treatment<sup>41</sup>.

TEMPO (2,2,6,6-tetramethylpiperidine-1-oxyl) oxidation selectively converts primary hydroxyl groups on cellulose to carboxyl groups. The carboxylated cellulose fibers are subsequently mechanically disintegrated into nanofibers<sup>42,43</sup>. Wen et al. produced lignin-containing nanofibrils from high-yield poplar pulp using the TEMPO oxidation method followed by a high-pressure homogenization<sup>44</sup>. A reduction of lignin content was noticed with an increasing sodium hypochlorite (NaClO) amount since lignin could be partly oxidized and then depolymerized into water-soluble compounds during the oxidation process. The introduction of carboxyl groups has also been reported to reduce the thermal stability of the cellulose fibrils<sup>45</sup>.

### 1.3.3 Other treatments

Other treatments, such as organic acid hydrolysis, have also been used for nanocellulose production. Compared with inorganic acids, organic acids have the advantages of low corrosivity, mild reaction, and easy recovery<sup>46</sup>. In

addition, nanocellulose prepared by organic acid hydrolysis is shown to have higher thermal stability compared to that produced *via* sulfuric hydrolysis since the introduction of sulfate groups could act as the catalyst for cellulose thermal degradation<sup>47</sup>. This method has shown considerable advantages in realizing the large-scale production of lignin-containing nanocellulose materials.

#### **1.4 Overview of the production of nano/micro-cellulose films**

Different types of nanocellulose exhibit distinct properties, influencing their end applications. Cellulose nanocrystals, known for their high crystallinity and ability to form unique chiral nematic structure, are ideal for reinforcing nanocomposites and creating optical films<sup>48</sup>. However, the self-assembled CNC films tend to be brittle due to their lack of an energy-dissipating amorphous phase and their inability to form entangled networks<sup>49</sup>. In contrast, cellulose nano/microfibers are better suited for producing mechanically robust self-standing films<sup>50</sup>. Recently, the production of nano/micro-cellulose films has garnered significant interest due to their potential applications in various fields, such as packaging, biomedical devices, electronics, and wastewater treatment<sup>51–54</sup>. These films can be fabricated through multiple methods, and several factors, such as the preparation methods, filter media, and different drying techniques could influence the physicochemical properties of the resulting cellulose films<sup>55,56</sup>.

##### **1.4.1 Casting method**

In 1996, Dufresne et al. reported the preparation of cellulose microfibril films by a casting method from sugar beet pulps. Specifically, the suspensions were first put under a vacuum to avoid bubble formation and then cast into a plastic container and evaporated at 37 °C to obtain a uniform cellulose film<sup>57</sup>. Solution casting is one of the most straightforward methods for producing cellulose films. In this method, a cellulose suspension is prepared by dissolving or dispersing cellulose nano/microfibers in a suitable solvent, typically water or a mixture of water and organic solvents. The suspension is then poured into a mold or a flat surface and allowed to dry, forming a thin film. Isogai et al. produced self-standing composite films which are composed of Tempo-oxidized cellulose nanofibril (TOCNF) and anionic poly(acrylamide) (PAM) using a simple casting method and the composite films with different weight ratios of TOCNF and PAM were further investigated<sup>58</sup>. Wang et al. prepared a variety of nanocomposites of lignin-containing cellulose nanofibers and poly (lactic acid) (PLA) *via* a solvent-casting process<sup>59</sup>. In this method, the cellulose fibers gradually come into

contact during solvent evaporation and eventually agglomerate to form the cellulose films. The casting method to prepare cellulose films can achieve a 100% retention of cellulose fibers. The microstructures and compositions of produced nanocellulose films can also be easily adjusted<sup>60</sup>.

#### **1.4.2 Coating method**

The coating method used to produce nanocellulose films usually employs a substrate, allowing cellulose fibers to deposit on the surface of substrates and creating nanocellulose films with controlled thickness. Spin coating is one of the coating techniques used to produce cellulose films with nanometric thickness. Fortunati et al. assembled thin films of silver nanoparticles and cellulose nanocrystals on different substrates (gold, silicon, SiO<sub>x</sub>, and SiO<sub>2</sub>) by spin coating methods<sup>61</sup>. The impact of used substrates, deposition parameters, and modification of cellulose nanocrystals on the properties of the obtained films was studied, and results show that the simple spin coating along with an optimized substrate can alleviate the aggregation problem of nanoparticles, which are affected by the topography and roughness of used substrates. In another study, a sulfonic cellulose-grafted/graphene-coated Janus separator was constructed on one side of the commercial glass fiber separator through the spin-coating technique that can be applied for scalable production in energy storage systems<sup>62</sup>.

Recently, the spraying coating technique has also been reported to prepare nanocellulose coating on different substrates and free-standing nanocellulose films<sup>63,64</sup>. Different base surfaces can be used as substrates for deposition, including impermeable substrates like silicon wafers and stainless-steel plates or permeable substrates like paper sheets. Following the drying phase, the resulting film can be detached from the substrate<sup>65</sup>.

#### **1.4.3 Filtration method**

Filtration is another standard method for fabricating cellulose films, particularly for producing dense structures. The nanocellulose suspension is usually first diluted to a concentration of 0.01–1.0 wt% and then filtered through a membrane using a vacuum or pressure filtration device. At the same time, the cellulose fibers are deposited on the membrane surface. The wet film is then peeled off, and the final nano/micro-cellulose films are obtained after drying.

In 2008, Henriksson et al. produced microfibrillated cellulose with different average degrees of polymerization, and the corresponding cellulose films were

produced using a vacuum filtration method. The fiber suspension was first well stirred for good dispersion and then filtered on a glass filter funnel. Different filter membranes were used as the filtration medium for cellulose fibers with different degrees of polymerization<sup>50</sup>. Later, Sehaqui et al. reported a vacuum filtration method similar to a paper-making pattern, followed by supercritical CO<sub>2</sub> drying to produce porous nonwoven membranes composed of modified nanofibrillated cellulose fibers<sup>66</sup>. In another study, cellulose separators were fabricated using an undemanding paper-making-like process involving vacuum filtration; specifically, cellulose suspensions were filtered using a Büchner funnel through a nylon membrane at a reduced pressure. The as-prepared wet membrane with the nylon layer was then sandwiched between paper sheets and clamped between aluminum plates for further drying<sup>67</sup>. The filter size used in the preparation of cellulose films using the filtration method is a critical parameter, and one major disadvantage of this method is that cellulose fibers can not be completely retained during filtration. Traditional wire sieves have pore sizes much larger than the nanocellulose particles, leading to a low retention rate of cellulose fibers. Although filters with pore sizes in the range of 0.1–0.65 µm or smaller can significantly reduce the loss of nanocellulose particles, the water removal process can take several hours or even days depending on the charge and size of cellulose fibers<sup>52</sup>.

The casting method is advantageous for its simplicity. However, it is hampered by long drying times due to the slow evaporation of solvents. Achieving uniform film thickness over large areas can be difficult, and surface defects such as cracks, bubbles, or pinholes often arise during the drying process using the casting method. The spraying coating method offers versatility and the ability to coat large surfaces. However, it requires specialized spraying equipment and controlled environments. Achieving consistent film thickness can also be problematic using this method. The filtration method is notable for its ability to produce films with controlled thickness, which is advantageous for targeted applications sensitive to thickness, such as separators for batteries. However, it is often a slow process depending on the size and charge of cellulose fibers and the pore size of the filter, limiting the production throughput<sup>56,65</sup>.

## **1.5 Thesis aim and objectives**

This thesis systematically investigates the production and application potential of lignin-rich microfibrillated cellulose produced from high-kappa number kraft pulp, aiming to deepen our understanding of how the characteristics of raw

fibers and fabrication conditions influence the properties of lignin-containing microfibrillated cellulose films targeted for specific high-value applications, such as energy storage devices and wastewater treatment. This work seeks to optimize the utilization of abundant lignocellulosic resources by exploring these connections in the following sub-projects.

- In paper I, lignin-rich microfibrillated cellulose fibers were derived from unbleached softwood kraft pulps with high kappa numbers compared to lignin-free counterparts from fully bleached softwood pulp. The effects of residual lignin and drying conditions on the properties of the resulting lignin-containing microfibrillated cellulose films are thoroughly examined (Paper I).
- This study further delves into the impact of the chemical composition and morphological characteristics of raw fibers on the mechanical fibrillation process and performances of produced LMFCs. Additionally, the relationship between lignin structures, fiber morphology, and the properties of the lignin-rich cellulose films is explored to establish the structure-property relationship between raw fibers and produced LMFC films, and their failure mechanisms are further examined (Paper II).
- Further investigation focuses on the effects of hot-press treatments on the wet strength of the produced LMFC films, and their potential as environmentally friendly separators for aqueous zinc-ion batteries is assessed in comparison with commercial Celgard separators (Paper III).
- Paper IV evaluates the potential of using lignin-rich microfibrillated cellulose films as adsorbents for removing cationic organic dyes, specifically methylene blue and crystal violet. The influence of residual lignin and the origin of LMFC films on their adsorption capacity is studied. The effect of pH and ionic strength on their adsorption performance and the adsorption capacities of dyes from both simulated and actual wastewater samples are examined. Additionally, Paper V investigates the gas transport and proton conductivity of the produced lignin-containing MFC membranes designed as proton-exchange membranes. The impact of residual lignin, membrane thickness, relative humidity, and operating temperatures on the proton conductivity of produced LMFCs is thoroughly studied.

A better understanding of these relationships will allow us to control the choice of raw materials and processes for obtaining lignocellulosic nano/micromaterials with desirable properties for targeted applications. The insights gained from this research can significantly contribute to the sustainable development of lignocellulosic nano/micromaterials, thereby broadening the range of potential applications for environmentally friendly nanocellulose materials.

## **1.6 Sustainability**

Producing lignin-rich microfibrillated cellulose films from high-kappa number kraft pulps aligns closely with several United Nations Sustainable Development Goals (SDGs), particularly related to sustainable industry, climate action, and responsible consumption and production<sup>68,69</sup>. Utilizing unbleached pulps, which retain a high lignin content, is an eco-friendly approach that minimizes the need for harsh chemical treatments typically used in the delignification process. This reduces the environmental impact of the pulp and paper industry and introduces unique properties to MFC films, making them suitable for various applications<sup>5</sup>.

The development of lignin-rich MFC films from unbleached pulps represents a significant advancement in sustainable materials science, contributing to SDG 9, which emphasizes the importance of building resilient infrastructure and fostering innovation. Lignin-rich MFC films are a biodegradable and renewable alternative to synthetic materials, reducing reliance on petroleum-based materials and promoting more sustainable solutions for various applications. Using sustainable wood-based materials for wastewater treatment is also in favor of SDG 14, which aims to protect life underwater by reducing marine pollution and protecting marine ecosystems. This thesis also contributes to SDG 12 by introducing an industry-scalable and chemical-free production pattern of lignin-rich cellulose materials, contributing to the responsible consumption and production goals.

The recyclability of these films supports a circular economy pattern by promoting resource efficiency, waste reduction, and sustainable production. A circular economy aims to eliminate waste and promote the continual use of resources<sup>70</sup>. Recyclable cellulose films support this model by ensuring materials are reused, remanufactured, and recycled rather than disposed of after a single use. This further contributes to the sustainability goal SDG 13, “Climate action”, as it helps lower carbon emissions by reducing the energy consumption

associated with producing new materials, thereby contributing to global efforts to mitigate climate change. It also supports SDG 12 by reducing the need for raw materials and promoting sustainable production practices.

## 2 Materials and methods

### 2.1 Materials and chemicals

The fully bleached softwood kraft pulp (mixture of spruce and pine) with a kappa number 2 was kindly provided by SCA. Lignin-rich softwood kraft pulp (Kappa number 64) derived from Scandinavian pine and hardwood kraft pulp (Eucalyptus) with a kappa number 96 were provided by Valmet AB and used as the starting materials. These three pulps were denoted as BSKP, LSKP, and LHKP, respectively.

### 2.2 Experimental methods

#### Preparation of MFC and LMFC gels

Alkaline washing was done according to Oliaei et al<sup>28</sup>. All pulp samples were washed to Na<sup>+</sup> form for better-swelling properties using Na<sub>2</sub>CO<sub>3</sub>. The never-dried pulp was then refined in a laboratory PFI mill refiner at 30000 revolutions. Subsequently, all pulp samples were mechanically defibrillated using a stone disk grinder Supermasscolloider (MKZA 10-15J CE IV) at 1500 rpm for 10 passes respectively. The grinder contains a pair of rotary and stator stone disks. Pulp fibers were pushed through the gap between the disks and underwent repeated cyclic pressure and shearing forces, converting the macro material into micro- and nano-sized particles.

#### Preparation of MFC and LMFC films

Following the microfibrillation process, MFC and LMFC gels were diluted to 0.2 wt% and dispersed with an Ultra Turrax mixer for 10 min at 12000 rpm. All films were fabricated using vacuum-assisted filtration methods. Specifically, well-dispersed MFC and LMFC suspensions were degassed and filtered *via*

vacuum filtration using a 0.65  $\mu\text{m}$  DVPP membrane (Durapore). The subsequent film was then sandwiched between another DVPP membrane and a paper sheet and dried in Rapid Köthen sheet former. Two drying conditions were tested in Paper I:  $93 \pm 2$  °C and  $40 \pm 2$  °C with a pressure of  $95 \pm 3$  KPa in Rapid Köthen sheet former. After drying, the MFC and LMFC films were conditioned at  $23 \pm 2$  °C and 50% relative humidity for at least 24 h before any measurements.

## **2.3 Characterization techniques**

### **Chemical composition**

Acid hydrolysis is a fundamental method for deconstructing complex carbohydrates in pulps into monosaccharides. By breaking down cellulose and hemicellulose, acid hydrolysis facilitates the quantification of monosugars such as glucose, xylose, arabinose, mannose, rhamnose, and galactose, which allows for a precise determination of the cellulose and hemicellulose content in the sample. An anion-exchange chromatography Dionex ICS-3000 (HPAEC-PAD) was used to analyze the soluble monosaccharides, including arabinose, galactose, glucose, xylose, mannose, and rhamnose. The acid-insoluble residue, also known as the Klason lignin, was determined gravimetrically. The Kappa number of all samples was measured according to ISO 302:2015 (E) standard.

### **Pulp fiber morphology**

Lorentzen & Wettre (L&W) Fiber Tester was used to characterize the morphology of pulp fibers, such as fiber length, width, shape factor, and number of kinks<sup>71</sup>. Pulp fibers were analyzed in a water suspension using an imaging system, and the morphology parameters were retrieved from the images of the diluted pulp samples.

### **Py-GC/MS analysis**

The Py-GC/MS analysis was performed using a Frontier Lab (Fukushima, Japan) Micro Double-shot Pyrolyser Py-2020iD, coupled with a Shimadzu GC/MS-QP 2010 apparatus with a capillary column RTX-1701 (Restec, USA) following the reported protocol<sup>72,73</sup>. The molar areas of the relevant peaks were summed and normalized to 100%, with data averaged from three repeated pyrolysis experiments.

### **Fiber total charge**

Total charge refers to the overall electrostatic charge on pulp fibers and fines, which is important in papermaking and nanocellulose production<sup>74–76</sup>. The total charge or total carboxylate content of fibers was evaluated using a Metrohm titrator (Titrino 702 SM Metrohm AG, Herisau, Switzerland)<sup>77</sup>. Pulp samples were protonated first into H<sup>+</sup> and titrated against 0.1M NaOH<sup>78</sup>. All data was processed using Tiamo 2.3 software.

The carboxylate content of fibers was calculated based on the volume of 0.1M NaOH solution needed to neutralize carboxyl groups following the equation:

$$\text{Carboxylate content } (\mu\text{mol/g}) = \frac{(V_2 - V_1)}{m} \times 0.1 \text{ M NaOH} \times 1000 \quad (1)$$

V<sub>2</sub>-V<sub>1</sub> is the volume of NaOH consumed, and m (g) is the sample weight on a dry base.

### **Surface charge measurement**

The surface charge measurement was done using stabino polyelectrolyte titration by titrating the dispersed fibers in Na<sup>+</sup> form. Cationic Poly-DADMAC with a charge of 0.345 μeq mL<sup>-1</sup> was used as the titration reagent<sup>74,75,79</sup>. The molecular weight of the polyelectrolyte is between 400k-500k g/mol.

### **Thermogravimetric analysis**

The thermal properties of all samples were characterized using thermogravimetric analysis (Mettler Toledo TGA/DSC instrument coupled with a STARe System). The tests were conducted with a heating range from 30 °C to 700 °C and a heating rate of 10 °C min<sup>-1</sup> under a nitrogen atmosphere. A nitrogen flow rate of 50 mL min<sup>-1</sup> was used in all TGA measurements.

### **Fourier transform infrared measurement**

Fourier Transform Infrared (FTIR) spectroscopy was employed to analyze the chemical structures of MFC and LMFC films. Measurements were conducted using a Perkin-Elmer Spectrum 100 FTIR spectrometer equipped with a Golden Gate single-reflection ATR accessory. The spectra were recorded over a wavelength range of 4000–600 cm<sup>-1</sup>, accumulating 16 scans per sample at a resolution of 4 cm<sup>-1</sup> at room temperature.

### **Contact angle measurement**

The static contact angle was measured using a Theta Lite contact angle analyzer (Biolin Scientific, Finland). The contact angle was recorded after 10 seconds, and the data was processed using One Attension software.

### **Mechanical properties**

The thickness of all films was measured using a Mitutoyo S112SB thickness tester, with measurements taken at a minimum of 10 points on each film, and the average was reported. Film density was calculated based on the weight and geometric dimensions. For tensile testing, strips with dimensions of 5 mm in width and 55 mm in length were cut from each film. The test was performed using an Instron 5944 instrument with a video extensometer. The gauge length was 25 mm, and a constant elongation rate of 5 mm min<sup>-1</sup> was used.

### **SEM characterization**

The surface and cross-section morphology of all films were characterized using a Hitachi S-4800 field-emission scanning electron microscope. All samples were cut and then sputter-coated with a platinum-palladium layer using a 208HR Cressington Sputter Coater (Cressington Scientific Instruments, Watford, UK).

### **Digital image correlation (DIC)**

Digital Image Correlation is a non-contact optical technique used to measure full-field surface displacements and strains in materials or structures<sup>80,81</sup>. To study the strain distribution on the produced samples, the surfaces of samples were sprayed with random white speckle patterns first to manifest deformation information during tensile tests. All samples are loaded with a constant speed of 5 mm min<sup>-1</sup>. The images of the sample were recorded using a stereo-digital image correlation (stereo-DIC) system equipped with two Basler acA4096-30um cameras (resolution of 4096 × 2168 pixels) at a frequency of 5Hz/s. The recorded images were processed using VIC-3D (Correlated Solutions, USA), and the subset size is 31 × 31 pixels, step size of 5 pixels, and strain window size of 11 × 11 points.

### **Wet tensile test**

All samples were immersed in deionized water for 48 hours before the wet tensile testing. The thickness of the wet strips was measured by placing a glass slide between the sample and the thickness tester to prevent excessive compression from the tester's tip on the wet surface. The wet mechanical

properties of the samples were then evaluated using a constant elongation rate of 5 mm min<sup>-1</sup>. Notably, these tests were conducted without the use of a video extensometer.

### **Porosity measurement**

The porosity of the separators was determined using an n-butanol impregnation method as described by Cao et al.<sup>82</sup> in Paper III. Separators with the same diameters were immersed in n-butanol for 1 hour, and their mass change was recorded. The porosities of all samples were calculated based on the following equation<sup>82,83</sup>.

$$\text{Porosity} = \frac{\Delta m}{\rho V} \quad (2)$$

In this equation,  $\Delta m$  represents the mass change of each separator before and after soaking in n-butanol,  $\rho$  is the density of n-butanol, and  $V$  is the volume of the separators.

### **Electrochemical characterization**

The symmetrical cells, comprising stainless steels (SS), were assembled by putting an electrolyte-saturated separator between two SS electrodes in the cells. The assembled cells were then utilized for the electrochemical impedance spectroscopy (EIS) measurements with a frequency range of 0.1 Hz to 100 kHz. The corresponding ionic conductivity ( $\sigma$ ) was calculated using the resistance values derived from the EIS spectra according to the following equation:

$$\sigma = \frac{L}{R \times S} \quad (3)$$

where  $L$  represents the separator thickness,  $R$  denotes the bulk resistance obtained from the EIS spectra, and  $S$  is the effective area of the separator<sup>84</sup>.

The performance and durability of various separators were further evaluated using galvanostatic charging/discharging cycling tests. Symmetrical cells with zinc electrodes were assembled, utilizing MFC, LMFC, MFC-HP, LMFC-HP, and Celgard 3501 as separators, each placed between zinc foils (99.99% purity, 1 mm thickness, Hauner GmbH). An alkaline electrolyte solution comprised of a mixture of 4 M KOH, 2 M KF, and 1 M K<sub>2</sub>CO<sub>3</sub><sup>85</sup> was used. The cells were assembled under atmospheric conditions and tested at room temperature.

### **Adsorption study**

The adsorption performances of membranes were evaluated using two cationic dyes, methylene blue (MB) and crystal violet (CV), *via* batch adsorption

experiments. Membrane samples, cut into 5 mm × 5 mm pieces and weighed to 2.5 mg (equivalent to an adsorbent dosage of 0.5 g L<sup>-1</sup>), were placed in flasks containing dye solutions of specified compositions. These flasks were shaken using an Orbital Shaker (INC/REFRIG 5000IR) at a constant speed of 130 rpm and at 25 °C for 5 h (the shaking time is varied in the kinetics study). After adsorption, the residual dye concentrations in the solutions were measured using a UV-3100PC spectrophotometer at 664 nm for MB and 590 nm for CV.

The amount of dye adsorbed per unit mass of membrane ( $q$ , μmol g<sup>-1</sup>) and the removal efficiency ( $R$ , %) were then calculated using the following equations:

$$q = \frac{C_i - C_e}{m_s} \times V \quad (4)$$

$$R = \frac{C_i - C_e}{C_i} \times 100\% \quad (5)$$

where  $C_i$  and  $C_e$  refer to the dye concentrations (μmol L<sup>-1</sup>) at the initial and equilibrium states, respectively,  $m_s$  (g) denotes the mass of the membrane and  $V$  (L) is the volume of the initial solution. All tests were repeated at least three times.

The influence of pH on dye adsorption was examined using Britton-Robinson buffer (BRb, 0.02 mol L<sup>-1</sup>) across a pH range of 5 to 7. The desired pH value was achieved by adding 1 mol L<sup>-1</sup> NaOH. The effect of ionic strength was evaluated by adding KCl (0.25 – 0.75 mol L<sup>-1</sup>). Adsorption kinetics were evaluated from 15 min to 24 h. The dye concentrations were 24.5 μmol L<sup>-1</sup> for MFC-SW and 73.6 μmol L<sup>-1</sup> for both LMFC-SW and LMFC-HW samples. No buffer was used for the above experiments. The practical applicability of the synthesized membranes was assessed in both simulated and real water systems: simulated groundwater (SGW) with a pH of 6.5 and actual river water (ARW) from the Fyris River in Uppsala, Sweden, with a pH of 7.5. The concentration of each dye was 4 μmol L<sup>-1</sup>, and the absorbance of solutions was registered within 380 – 800 nm.

### Proton conductivity measurement

The proton conductivity of the fabricated membranes was evaluated at different temperatures and relative humidity using a membrane testing device (MTS-740, Scribner Associates, Southern Pines, NC, USA) connected to an impedance spectroscopy analyzer (MFIA 500 kHz, Zurich Instruments, Switzerland). Impedance spectra were recorded with an AC amplitude of 10 mV, covering a frequency range from 0.5 MHz to 1 Hz. For a standard test, impedance was measured at a constant temperature while RH was

incrementally adjusted from 20% to over 95%. For temperatures above 100 °C, the measurement chamber was back-pressurized at 230 kPa.

### **Gas permeability test**

The permeation measurements of dry pure gases (H<sub>2</sub>, CO<sub>2</sub>, N<sub>2</sub>, and O<sub>2</sub>) were conducted using the differential pressure method (GTR-11A/31A, GTR-TEC Ltd., Japan). In this setup, gas transport through the membrane is driven by a vacuum on the permeate side and an applied pressure on the feed side. The amount of gas permeating through the membrane was quantified using gas chromatography (Yanaco G3700T, Fukuoka, Japan), and each sample was measured in multiple replicates. The test cell and part of the feed gas delivery system were kept at a controlled temperature of 35 °C. A Kapton tape gasket was used to mask the membrane, allowing gas permeation through a specific area (diameter = 1 cm, area = 0.785 cm<sup>2</sup>). All measurements were performed under a total pressure difference of 300 kPa. The selectivities for different gas pairs were determined by the ratio of permeabilities,  $\alpha_{x/\gamma} = P(X)/P(Y)$ , where X and Y represent the fast and slow permeating gases, respectively.



### 3 Results and discussion

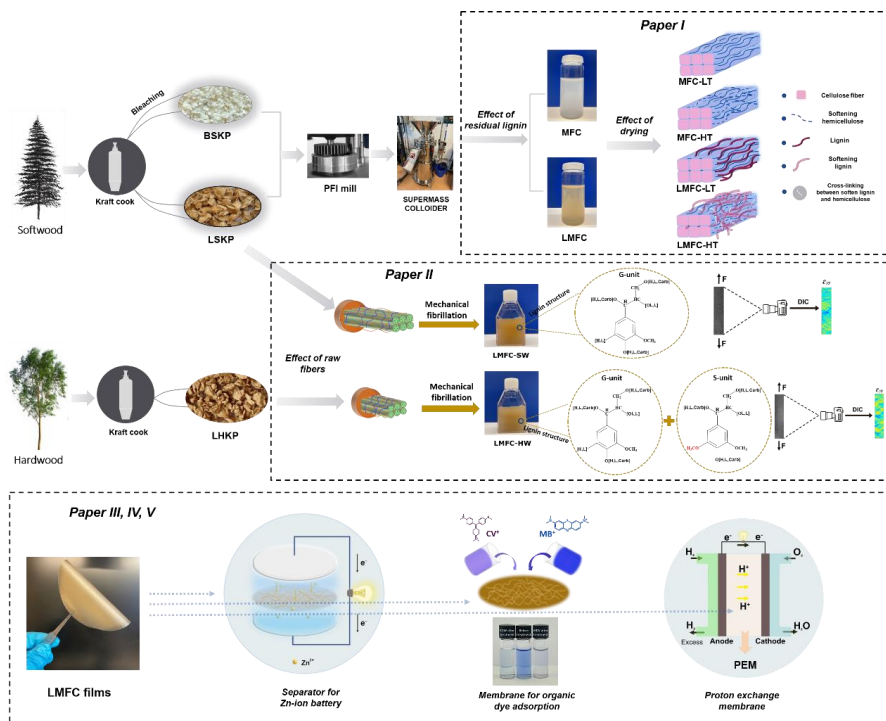


**Figure 2.** An illustration of the work in the appended papers included in the thesis.

This thesis focuses on the production and applications of lignin-rich microfibrillated cellulose fibers. The aim is to enhance our understanding of the connections between raw fibers, fabrication conditions, and the properties of produced lignin-containing microfibrillated cellulose for specific applications to

achieve value-added utilization for abundant lignocellulosic materials. An illustration of the work included in this thesis is presented in Figure 2.

### 3.1 Characterization of raw pulps

In this project, three different pulps were used as raw materials to produce lignin-free and lignin-rich nano/micro-cellulose fibers. The characteristics of raw fibers are of great significance as they would affect the mechanical fibrillation process and final properties of produced cellulose nano/microfibers. The chemical composition of three different raw pulps was determined using the acid hydrolysis method, and the results are presented in Figure 3.

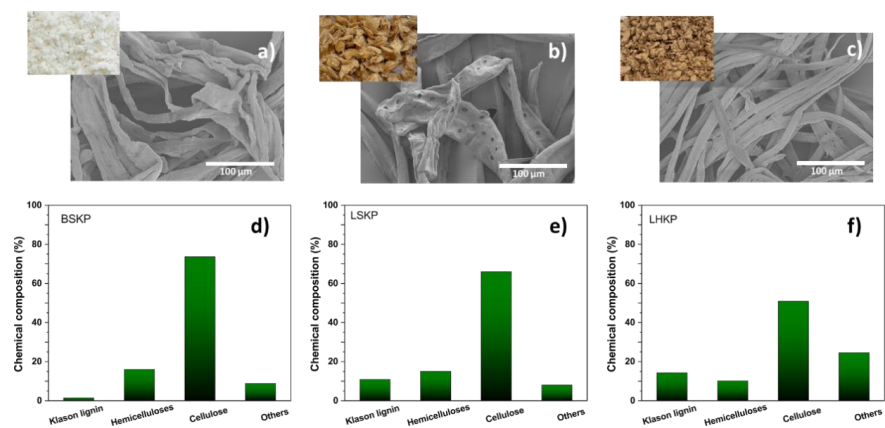


**Figure 3.** Photos and SEM images of raw pulps a) BSKP, b) LSKP, and c) LHKP; Chemical compositions of raw pulps d) BSKP, e) LSKP, and f) LHKP (Figure adapted from Paper IV).

As can be seen from Figure 3, the three pulps showed different physical appearances. LSKP and LHKP exhibit a brown color due to residual lignin. Fully bleached softwood kraft pulp BSKP displays a more curled shape with a higher curl index presented in Table 1 than unbleached softwood pulp. This is attributed to the longer pulping time and to the chemical treatments used during bleaching<sup>86</sup>. The removal of lignin, which plays a crucial role in supporting fiber cell wall structures, leads to the collapse of pulp fibers. The SEM images in Figure 3 further illustrate the morphological differences between softwood and hardwood pulp fibers. Softwood pulp fibers are generally longer, thicker, and have a higher aspect ratio (length-to-width ratio) than hardwood pulp fibers<sup>87</sup>. The unbleached softwood pulp fibers are 2-3 times longer and nearly twice as wide as unbleached hardwood pulp fibers, as detailed in Table 1.

Softwood and hardwood pulp fibers also differ in their chemical compositions. Both pulp fibers consist of cellulose, hemicellulose, and lignin, but the proportions of these components vary. The bleaching process effectively removed most residual lignin components, resulting in only about 1% Klason lignin remaining in BSKP, as seen in Figure 3d. In contrast, LSKP and LHKP retained high levels of Klason lignin of around 11% and 14%, respectively.

**Table 1.** Pulp yield and pulp fiber parameters.

Samples	Pulp Yield (%)	Pulp fiber parameters				
		Mean length (mm)	Mean width ( $\mu\text{m}$ )	Mean shape factor (%)	Curl index (%)	Number of kinks per fiber
<b>BSKP</b>	47.0	1.93	30.1	79.6	25.6	1.38
<b>LSKP</b>	54.6	2.52	36.7	91.5	9.3	0.30
<b>LHKP</b>	70.7	0.95	21.9	93.3	7.2	0.23

In this study, microfibrillated cellulose and lignin-containing microfibrillated cellulose were produced from fully-bleached and unbleached kraft pulps employing chemical-free treatments. All pulp fibers were initially refined using a laboratory PFI mill, followed by mechanical defibrillation with a Supermasscolloider, avoiding chemical pretreatments such as TEMPO-oxidation or carboxymethylation to reduce the damage to the lignin structures and content<sup>44</sup>.

### 3.2 Effect of residual lignin

#### Effect of residual lignin on nano/micro-cellulose suspensions

To investigate the impact of residual lignin on the properties of lignin-rich microfibrillated cellulose, fully bleached softwood kraft pulp and high-kappa number softwood kraft pulp were utilized as sources for producing lignin-free and lignin-rich nano/micro-cellulose fibers. As illustrated in Figures 4a and 4b, both micro-sized fibers and nano-sized fibrils were observed in the MFC and LMFC gel suspensions, indicating a broad size distribution in the samples.

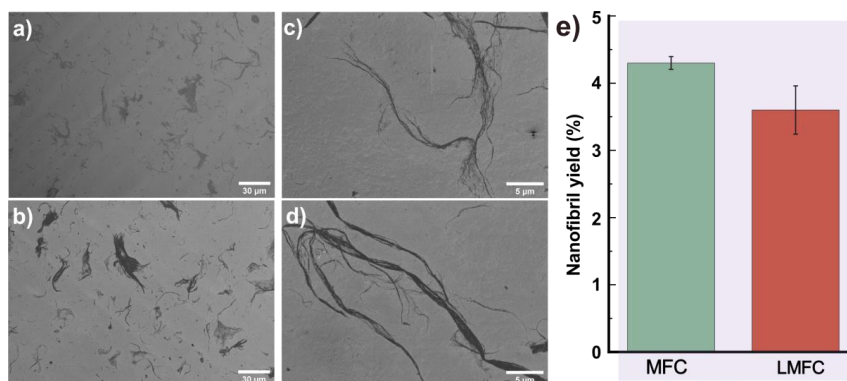


**Figure 4.** SEM images of a, c) MFC and b, d) LMFC suspensions; e) nanofibril yield of MFC and LMFC suspensions after fractionation (Figure adapted from Paper I)<sup>86</sup>.

The nanofibril yield for MFC and LMFC products was 4.3% and 3.6%, respectively (Figure 4e). The lower yield in LMFC samples can be attributed to the high lignin content of the raw pulps, as lignin likely acts as a binding agent within the cellulose fibers<sup>28,88</sup>, as well as the coarse grinding method. LMFC fibers demonstrated a higher surface charge, as shown in Figure 5b, which is associated with an increased number of carboxylic groups present in the lignin-rich fibers. This higher carboxyl content also led to a greater absolute zeta potential in LMFC gel suspensions than in MFC dispersions, as shown in Figure 5c, indicating enhanced colloidal stability in LMFC suspensions.

Remarkably, no significant sedimentation was observed in LMFC dispersions even after 100 days of incubation (Figure 5d). This stability is particularly advantageous for the commercial use of lignin-rich cellulose, as it reduces the need for intensive dispersion processes typically required to prevent fiber aggregation in MFC suspensions.

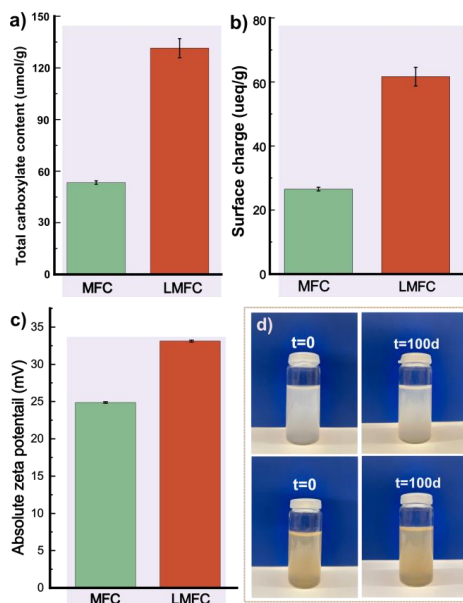


**Figure 5.** a) Total carboxylate content, b) surface charge, and c) absolute zeta potential of MFC and LMFC fibers produced from lignin-free and lignin-rich softwood kraft pulp; d) photographs of MFC and LMFC suspensions before and after 100 days of incubation (Figure adapted from Paper I)<sup>86</sup>.

#### Effect of residual lignin on physicochemical properties of nano/micro-cellulose films

Self-standing films were produced from MFC and LMFC suspensions to study the impact of residual lignin on the physicochemical properties of nano/micro-cellulose fibers. Figure 6 shows the morphology characteristics of MFC and LMFC films, both exhibiting a network of interconnected fibers. All films exhibit a lamellar structure, which can be clearly seen from the cross-section images. Some particles (as the arrow points) could also be observed at the fracture boundary of LMFC samples, which are likely residual lignin particles presented onto fibers<sup>89</sup>.

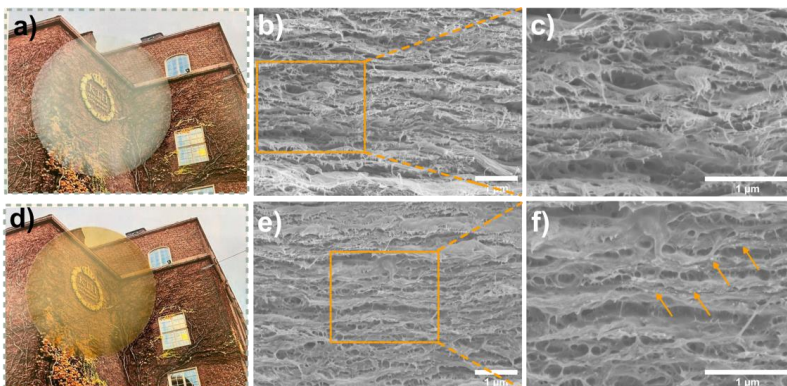


**Figure 6.** a) and d) Photos of MFC-HT and LMFC-HT films dried at elevated temperatures; SEM images of the cross-section morphology of b, c) MFC-HT and e, f) LMFC-HT films at different magnification (Figure adapted from Paper I)<sup>86</sup>.

Thermogravimetric analysis was employed to evaluate the thermal properties of MFC and LMFC samples, as well as the impact of residual lignin on the thermal properties of the resulting films<sup>90,91</sup>. Figures 7a and 7b show the weight loss curves of four samples and the corresponding derivative thermogravimetric curves. The initial weight loss observed between 30 °C and 120 °C is attributed to moisture evaporation, resulting from the absorbed water of fibers, while the primary degradation phase of samples occurs between 300 – 400 °C<sup>92,93</sup>. Lignin-rich cellulose films showed higher  $T_{\text{onset}}$  and  $T_{\text{max}}$  than those of lignin-free cellulose films. Furthermore, a higher percentage of the charred residue of LMFC remained after thermal decomposition. The improved thermal properties of lignin-rich MFC films could be attributed to the higher thermal stability of lignin than cellulose and hemicellulose<sup>94</sup>. Generally, lignin degradation occurs over a broader temperature range due to its complex composition and structure<sup>92</sup>. The aromatic groups and different ether bonds in lignin are essentially stable below 300 °C<sup>45</sup>. It has been reported that increasing the lignin content from 15.5% to 23.1% can further enhance the thermal stability of lignin-rich films<sup>44</sup>.

Lignin-rich cellulose films produced through a pure mechanical method demonstrated superior thermal stability ( $T_{\text{max}} > 345$  °C) compared to carboxymethylated CNF and TEMPO-oxidized CNF films reported by Kim et al.<sup>95</sup>. The introduction of carboxyl groups has been shown to reduce the thermal stability of nanocellulose<sup>45</sup>. Additionally, the reduced fiber dimensions and increased surface area of cellulose nanofibers render them more susceptible to heat-induced degradation<sup>91</sup>. Figure 7c displays the water contact angle of all

samples. Lignin endows more hydrophobic characteristics of LMFC samples as lignin is a more hydrophobic polymer due to the aromatic moieties<sup>96</sup>.

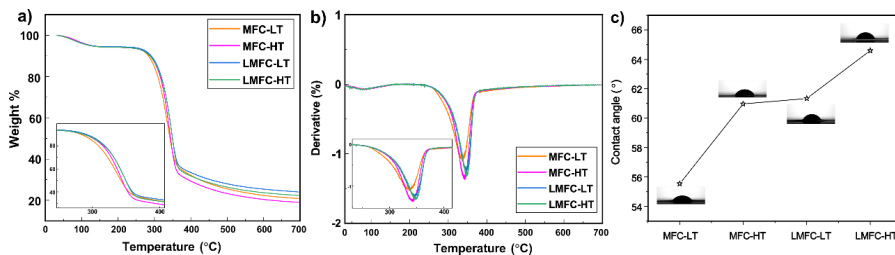


**Figure 7.** a) TGA and b) DTG curves of MFC-LT, LMFC-LT, MFC-HT, and LMFC-HT films with enlarged figures of main degradation curves; c) Water contact angle of all samples (Figure adapted from Paper I) <sup>86</sup>.

### 3.3 Influence of raw fibers

#### Effect of raw fibers on the defibrillation process

Unbleached softwood and hardwood kraft pulps with high kappa numbers were used to produce lignin-containing microfibrillated cellulose fibers to study the effect of raw fiber characteristics on the defibrillation process and the properties of final products. To assess the impact of different wood species on the fibrillation of high-lignin-content pulps, the surface charge of the softwood and hardwood intermediate products was measured across various defibrillation passes. Surface charge can serve as an indicator of the degree of fibrillation, as it correlates with the specific surface area and, consequently, the particle size of the cellulose fibrils<sup>79</sup>.

The surface charge of fibers derived from lignin-containing hardwood kraft pulp increased significantly between the 4th and 8th fibrillation passes as presented in Figure 8a, indicating their greater degree of fibrillation than softwood kraft pulp. This suggests that hardwood pulp fibers are more readily disintegrated than the softwood counterparts. This enhanced disintegration can be attributed to two primary factors: the smaller dimensions of the LHKP raw fibers and the higher fiber charge, which likely increases their susceptibility to external forces, thereby facilitating the breakdown of fibers into smaller fragments during the defibrillation process<sup>97</sup>.

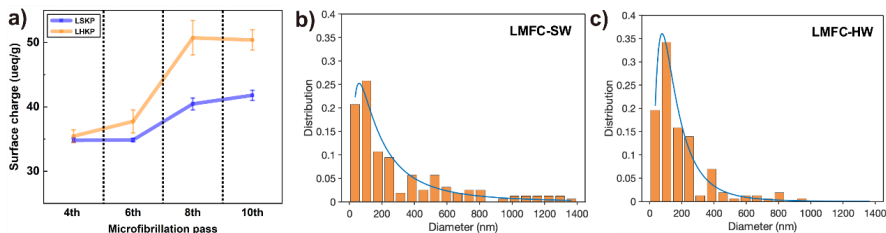


**Figure 8.** a) Surface charge of LSKP and LHKP fibers at different defibrillation passes; Diameter distribution of prepared b) LMFC-SW and c) LMFC-HW fibers (Figure adapted from Paper II) <sup>87</sup>.

Figures 8b and 8c show the size distribution of produced lignin-rich microfibrillated cellulose fibers derived from softwood and hardwood pulps after the 10th grinding pass. Both LMFC-SW and LMFC-HW exhibited a broad range of diameter distributions. When the diameter distribution was fitted to a log-normal model, the mean diameter and standard deviation were 74 nm and 69 nm for LMFC-SW and 53 nm and 57 nm for LMFC-HW, respectively. These results indicate that LMFC-HW fibers have a smaller average diameter and narrower diameter distribution than LMFC-SW fibers. This difference can be attributed to the lower fibrillation efficiency of LMFC-SW under the same energy input and the inherently smaller fiber dimensions of hardwood, which influence the size distribution of the resulting LMFC products.

Figure 9 presents the SEM images of softwood and hardwood pulp fibers after the 4th, 6th, 8th, and 10th grinding passes. Due to the high lignin content, which acts as a binder between cellulose fibrils in the raw material, few fibrillated fibers can be observed during the initial grinding stages. However, as a higher energy input was employed with increasing grinding passes, more free fibers were produced, as seen in Figures 9c and 9g. This trend aligns with the significant increase in surface charge observed between the 6th and 8th passes in Figure 8a, with a high degree of fibrillation achieved after the 6th pass.

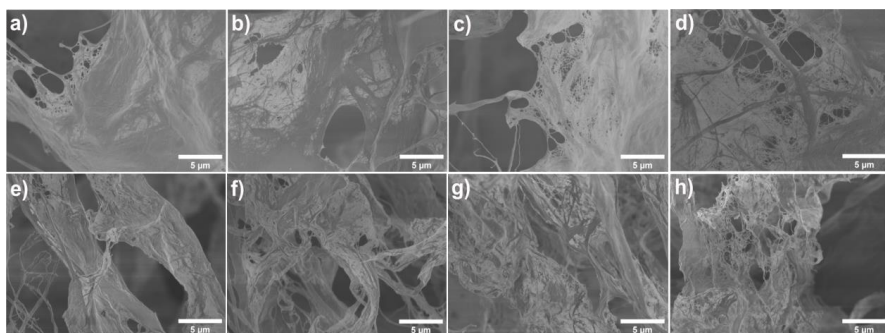


**Figure 9.** SEM images of a-d) LSKP and e-h) LHKP fibers at the 4<sup>th</sup>, 6<sup>th</sup>, 8<sup>th</sup>, and 10<sup>th</sup> grinding pass (Figure adapted from Paper II) <sup>87</sup>.

#### **Effect of raw fibers on mechanical properties of nano/micro-cellulose films**

The mechanical properties of lignin-rich microfibrillated cellulose fibers derived from various wood species were assessed by analyzing their performances as self-supporting films. Tensile strength tests were conducted on LMFC derived from softwood (LMFC-SW) and hardwood (LMFC-HW), with the results presented in Figure 10a. LMFC-SW exhibited a higher tensile strength of 288 MPa and a higher Young's modulus than LMFC-HW. To explore the mechanical behavior of high-lignin content cellulose films derived from different wood sources, a comprehensive study was undertaken to investigate how raw pulp fibers affect the properties of these lignin-rich microfibrillated cellulose films.

The uniaxial tensile behavior of LMFC-SW and LMFC-HW films was thoroughly examined using digital image correlation to characterize the failure mechanisms in the lignin-rich films. Figures 10b and 10c present the surface images of the samples at the onset and fracture point, respectively. The images were processed through a DIC algorithm to analyze the deformation, which enabled the extraction of full-field strain distributions across the sample surfaces during the tensile test. The tensile strain fields at 7.8 and 19.8 seconds are depicted in Figures 10e and 10f. The LMFC-HW samples exhibited pronounced regions of strain concentration, highlighted in red on the strain maps. These areas of intense localized strain indicate regions of lower modulus, likely due to insufficient fiber reinforcement and weaker fiber bonding. Conversely, regions depicted in blue correspond to higher modulus areas, indicating better fiber reinforcement and more uniform stress distribution across the films.

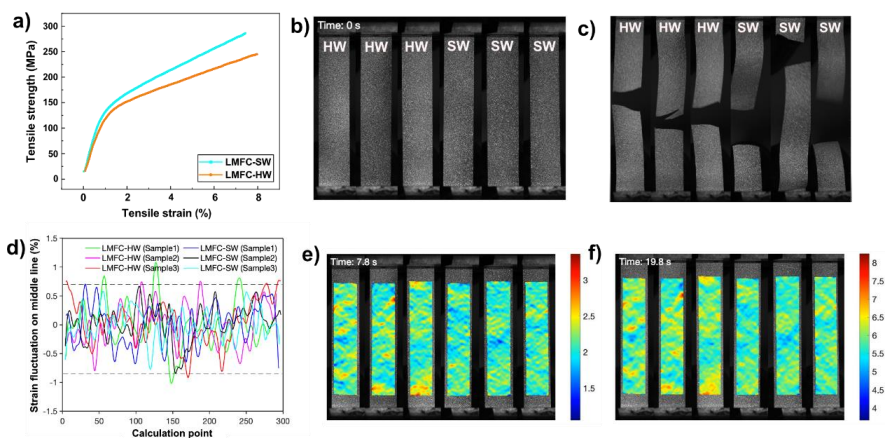


**Figure 10.** a) Stress-strain curves of LMFC-SW and LMFC-HW films; b) original specimen with speckle pattern; c) fractured specimen at the end of the tensile test; d) strain fluctuation along the vertical middle lines as recorded by DIC; e) strains at time 7.8 s, corresponding to tensile strain of 2.6%; f) strains at time 19.8 s, corresponding to tensile strain of 6.6% (Figure adapted from Paper II) <sup>87</sup>.

During tensile testing, LMFC-HW samples displayed more red regions, indicating more pronounced strain concentrations. This suggests that HW samples experienced less efficient stress distribution, which is evident at 7.8 seconds. On the contrary, LMFC-SW samples demonstrated better stress transfer across the samples with less strain concentration. By 19.8 seconds, this disparity became even more apparent: strain-concentrated regions in HW samples expanded significantly, while SW samples continued to exhibit a more uniform strain distribution under constant elongation. This improved performance in SW samples is likely due to more fiber bonding formed from the longer softwood fibers (Figure 11a) and the formation of more interconnected fiber networks by entangled fibers, as shown in Figure 11. These can enhance stress transfer during tensile loading, resulting in more uniform strain distribution within SW fiber matrices.

Comparing strain fields at 7.8 and 19.8 seconds, with applied strains of 2.6% and 6.6%, respectively, reveals that regions of strain inhomogeneity remained relatively stable, indicating that most of the observed deformation was due to fiber elongation and the tensile deformation did not significantly alter the material's microstructure. The strain fluctuation of films along the vertical middle lines was extracted (Figure 10d) to evaluate the strain inhomogeneity. LMFC-HW films show larger amplitudes of strain fluctuation on the strain curves, demonstrating the more significant strain inhomogeneity within HW

samples. Comparing the strain fields with fracture patterns, it was noted that HW samples fractured near the strain-concentrated regions. In contrast, SW samples fractured in regions that were not directly aligned with high local strain. Additionally, the crack in SW samples suggested a failure mode likely dominated by fiber breakage rather than the shear-dominated pull-out. This implies that the physical cross-linking between softwood fibers was strong, with the primary limitation being the inherent strength of the fibers themselves.

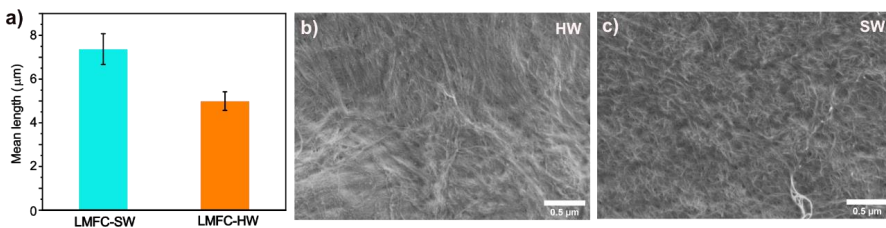


**Figure 11.** a) Mean particle size of LMFC-SW and LMFC-HW fibrils. SEM images of b) LMFC-HW and c) LMFC-SW films at high magnification (Figure adapted from Paper II)<sup>87</sup>.

The distinct chemical structures of lignin could also affect the final properties of lignin-rich films due to a significant portion of residual lignin in both LMFC-SW and HW films. Therefore, it is essential to understand the relationship between various lignin structures and their impact on the mechanical properties of lignin-rich films.

During the kraft pulping process, the structure of lignin undergoes substantial changes compared to its native form<sup>98</sup>. Native lignin is characterized by its complex networks, and  $\beta$ -O-4 linkages are prevalent in its structure. However, these linkages are significantly reduced in residual lignin after pulping due to their cleavage during the kraft process<sup>10</sup>. Analytical pyrolysis was employed to analyze the residual lignin structures in the raw pulps to understand how the distinct lignin structures from different wood species influence the mechanical properties of lignin-rich MFC films.

Table 2 presents the analysis of lignin derivatives in LSKP (softwood kraft pulp) and LHKP (hardwood kraft pulp) samples, focusing on phenyl, benzyl, guaiacyl, and syringyl derivatives. Phenyl and benzyl derivatives constitute 21.0% of the lignin content in the SW raw pulp, compared to only 7.2% in the HW raw pulp. HW samples exhibited a high proportion of syringyl derivatives, accounting for 73.2% of the lignin content, whereas the residual lignin in SW samples predominantly consisted of guaiacyl-based units. These differences

arise from the distinct monolignol compositions in softwood and hardwood lignins, specifically coniferyl alcohol in softwoods and sinapyl alcohol in hardwoods. Sinapyl alcohol-based lignin is less prone to forming condensed structures—where monolignols are linked *via* carbon-carbon bonds at the C5 position—due to a methoxy group at the C5 position in sinapyl alcohol that inhibits such coupling reactions. Consequently, LMFC-HW samples display fewer C5-condensed structures, reflecting the inherent differences in lignin structure between softwood and hardwood species. This structural variation could impact the mechanical performances of the resulting lignin-containing films.

**Table 2.** Classification of compounds obtained by Py-GC/MS of LHKP and LSKP (Table adapted from Paper II)<sup>87</sup>.

<b>Results/samples (% from chromatogram)</b>	<b>LSKP (%)</b>	<b>LHKP (%)</b>
<b>Lignin derivates (% from chromatogram)</b>	<b>5.44</b>	<b>19.45</b>
Phenyl and benzyl derivates	1.14	1.40
Guaiacyl derivates	4.30	3.81
Syringyl derivates	-	14.24
<b>Lignin derivates, 100%</b>		
Phenyl and benzyl derivates	20.96	7.20
Guaiacyl derivates	79.04	19.59
Syringyl derivates	-	73.21

As illustrated in Figure 10a, the LMFC-SW films demonstrated a higher elastic modulus of 15 GPa compared to 13 GPa of LMFC-HW films. This difference in stiffness is likely attributed to the synergistic effects of increased condensed C5 linkages and the preservation of longer fibers in the SW samples. The higher concentration of condensed C5 linkages in LMFC-SW, resulting from abundant guaiacyl units (Table 2), contributes to a more complex and rigid three-dimensional lignin structures. The dense, aromatic structure and reduced molecular mobility associated with these condensed C5 linkages enhance the stiffness of the material by restricting the free rotation between lignin monomers<sup>99</sup>. Moreover, the longer fibers of SW could further increase the stiffness of the films<sup>100</sup>. This further suggests that different raw materials can

significantly impact the mechanical properties of resultant lignin-rich cellulose films due to different lignin structures and fiber morphology displayed.

### 3.4 Effect of drying conditions

#### Effect of drying temperatures

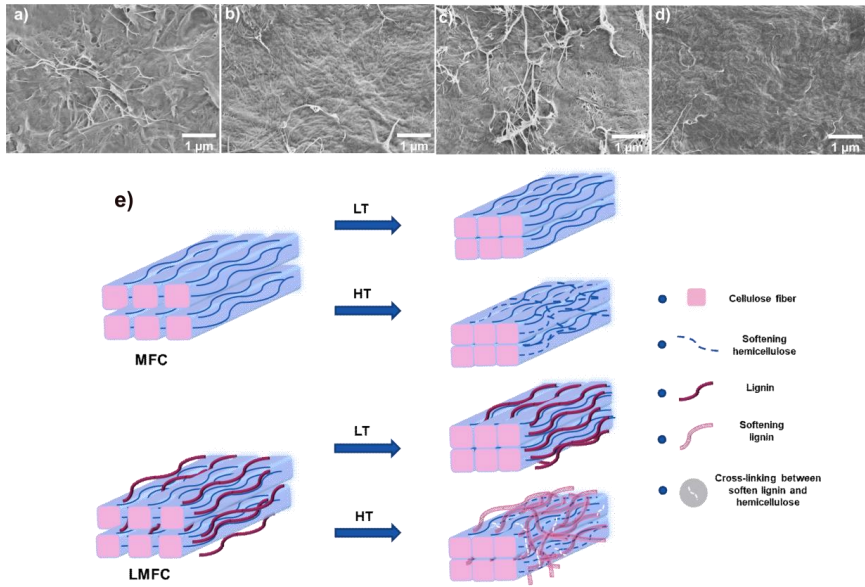


**Figure 12.** SEM images of surface morphology of prepared films using different drying temperatures a) MFC-LT, b) MFC-HT, c) LMFC-LT and d) LMFC-HT; e) Schematic illustration of MFC and LMFC films dried under different drying conditions (Figure adapted from Paper I)<sup>86</sup>.

It is demonstrated that the properties of amorphous wood polymers are correlated with environmental conditions. Specifically, lignin and hemicellulose, which are thermoplastic polymers, transition to a rubbery state under dry conditions at temperatures ranging from 180 to 220 °C. However, in the presence of water, the transition temperature of lignin can drop significantly (reaching 90 °C), while hemicelluloses soften at even lower temperatures<sup>101,102</sup>. Figures 12a-12d illustrate the surface morphology of both MFC and LMFC films, which exhibit a network of interconnected fibers. As drying temperatures increase, both lignin-rich and lignin-free films develop more compact structures. In MFC films, hemicelluloses begin to soften at elevated drying temperatures above 50 °C, whereas, in LMFC films, lignin could soften at

around 90 °C when in a wet state<sup>101,102</sup>, acting as filler between fibers and contribute to a denser surface structure.

The thickness, density, apparent porosity, tensile strength, and modulus of MFC and LMFC samples are presented in Table 3. Both films exhibited a slight increase in density at higher drying temperatures, consistent with the formation of more compact structures as observed through SEM. Notably, both MFC and LMFC films demonstrated excellent tensile strength, exceeding 220 MPa. Higher drying temperatures enhanced the Young's modulus and tensile strength of both lignin-free and lignin-rich films. This enhancement was particularly pronounced in LMFC samples, suggesting that lignin softens and effectively bridges the fibers after reaching the glass transition temperature, creating more fiber joints within the cellulose fiber networks, which is manifested in the improved modulus and tensile strength<sup>103</sup>.

**Table 3.** Physical and mechanical properties of MFC and LMFC films dried under different temperatures (Table adapted from Paper I)<sup>86</sup>.

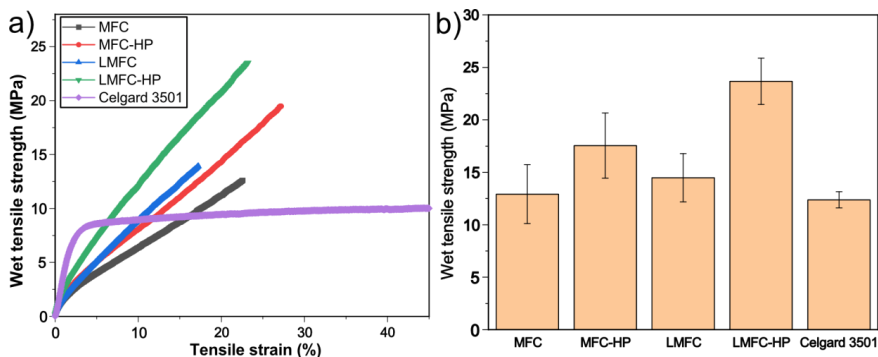
Samples	Thickness (μm)	Grammage (g/m <sup>2</sup> )	Density (g/cm <sup>3</sup> )	Apparent porosity (%)	Tensile strength (MPa)	Strain at break (%)	Young's modulus (GPa)
MFC-LT	26.0 ± 0.8	35.7 ± 1.1	1.37 ± 0.01	8.5 ± 0.9	228.8 ± 14.9	9.9 ± 0.4	8.96 ± 0.82
MFC-HT	24.2 ± 0.9	34.0 ± 1.2	1.40 ± 0.01	6.5 ± 0.7	240.8 ± 10.8	8.3 ± 0.9	14.57 ± 0.71
LMFC-LT	27.5 ± 0.6	37.2 ± 0.7	1.36 ± 0.01	9.6 ± 0.9	248.4 ± 13.1	10.3 ± 1.1	8.32 ± 0.69
LMFC-HT	25.2 ± 1.0	35.5 ± 1.2	1.41 ± 0.01	6.3 ± 0.9	282.7 ± 9.1	7.4 ± 0.7	15.06 ± 0.35

Figure 12e illustrates the mechanism underlying the enhanced tensile strength of MFC and LMFC films as drying temperatures increase. When these films are dried in a wet state, water acts as a plasticizer to soften and thereby lower the transition temperatures of hemicellulose and lignin. In lignin-free films, the softened hemicellulose fills the inter-fibril spaces, enhancing the fiber bonding between cellulose fibrils<sup>104,105</sup>. In lignin-rich films, the presence of water and elevated drying temperatures lead to the softening of lignin components. This softening activates the molecular mobility of lignin, enabling it to act as a cross-linker between cellulose fibers. As lignin softens, it deforms

more readily to conform to the configuration of fiber joints<sup>106,107</sup>. This contributes to a better stress transfer between cellulose fibers in the network structures.

### Effect of hot-press treatment

The impact of hot-press treatment on the mechanical performance of produced microfibrillated cellulose films is investigated. As illustrated in Figure 13, lignin-rich films exhibited better wet mechanical strength than lignin-free MFC films. This enhanced performance is attributed to the residual lignin, which contributes to a more robust fiber network and improved structural integrity<sup>72,88,108</sup>. Furthermore, both MFC and LMFC films demonstrated increased wet mechanical strength and greater tensile strain at break after hot pressing. Specifically, the wet mechanical strength of LMFC films rose significantly from approximately 14 MPa to 24 MPa after hot pressing, as shown in Figure 13b. The marked improvement in wet mechanical strength after hot pressing is likely due to the formation of a greater number of joints within the fiber network, leading to more effective load distribution<sup>109</sup>. The hot-press treatment is reported to facilitate cross-linking between lignin and the cellulose matrix through enhanced intermolecular interactions, thereby reinforcing the cellulose network and amplifying lignin's role as a structural binder<sup>108,110</sup>.



**Figure 13.** a) Stress-strain curves of wet samples and b) wet tensile strength of prepared films and commercial Celgard 3501 (Tests were done without video extensometer) (Figure adapted from Paper III).

### 3.5 Applications of lignin-rich nano/micro-cellulose films

#### Separators for aqueous zinc-ion battery

Aqueous zinc-ion batteries (AZIBs) have gained considerable attention in recent years due to their numerous advantages, including enhanced safety from using aqueous electrolytes, easy manufacturing process, non-toxicity, high volumetric capacity, and, notably, their cost-effectiveness<sup>111–113</sup>. Separators are crucial for ensuring the high performance of AZIBs, as they serve as physical barriers between the electrodes while also facilitating ion transport. Although separators are not electrochemically active components, they play a pivotal role in determining the energy density, power density, cycle life, and overall safety of the batteries. Motivated by the outstanding mechanical properties and cost-effectiveness of lignin-rich microfibrillated cellulose films. The electrochemical performances of utilizing lignin-rich MFC films as separators for AZIBs were further investigated in comparison with commonly used commercial Celgard separators.

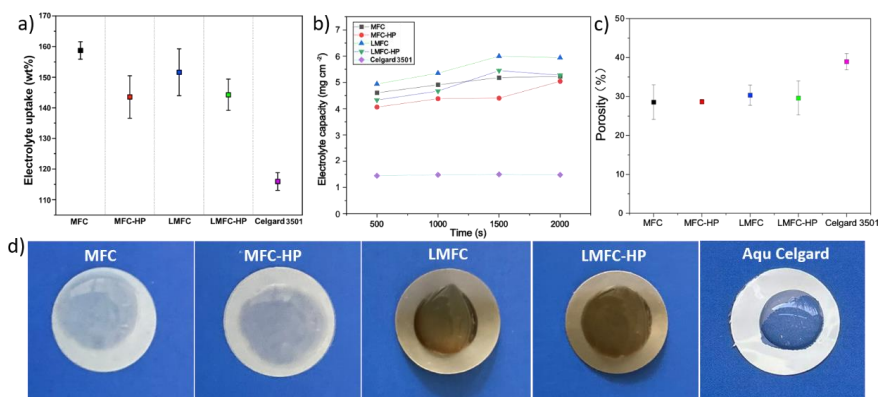


**Figure 14.** a) Electrolyte uptake and b) dynamic curves of electrolyte capacity of MFC, MFC-HP, LMFC, LMFC-HP films, and Celgard 3501; c) porosity of separators determined by n-butanol method; d) digital photos of MFC, MFC-HP, LMFC, LMFC-HP films, and Celgard 3501 with a drop (60  $\mu$ L) of electrolyte on the surface after 10s (Figure adapted from Paper III).

Electrolyte uptake and wettability are crucial factors that determine the performance of battery separators. Enhanced electrolyte uptake ensures that the separator can retain sufficient electrolyte, which is vital for efficient ion transport between electrodes and facilitates the effective charging and discharging of the battery<sup>114</sup>. As shown in Figure 14a, MFC shows the highest

electrolyte uptake at 159 % and 152 % for LMFC separators, both of which are higher than Celgard 3501, which shows an uptake of 116%. The higher hydrophilicity and swelling ability of cellulose fibers promote better wettability and uptake of aqueous electrolytes on cellulose-based separators compared to polyolefins. After the hot press, the electrolyte uptake of both MFC and LMFC separators decreased, likely due to the formation of denser structures within the cellulose-based films. The dynamic electrolyte capacity curves, shown in Figure 14b, follow the same trend. Celgard separators exhibited the lowest electrolyte capacity and remained almost unchanged over time; MFC-HP and LMFC-HP separators demonstrated a significant increase in electrolyte capacity, reaching up to 5 mg cm<sup>-2</sup> after 30 minutes of soaking. This further underscores the superior electrolyte-absorbing ability of cellulose-based separators. Figure 14d further illustrates the fast electrolyte diffusion on the surfaces of cellulose-based films.

The porosity of all separators was assessed using the n-butanol impregnation method<sup>83</sup> (Figure 14c), revealing that Celgard possesses higher porosity compared to cellulose-based materials. Porosity is a key parameter as pores not only function as electrolyte storage space but also provide channels for ion transport between the electrodes<sup>114</sup>. Figure 15 shows the surface morphology of Celgard 3501 designed for the aqueous battery, where more prominent micropores are visible. However, despite the higher porosity, the capacity of these larger micropores to retain liquid is lower compared to smaller pores. This is because smaller pores can achieve higher Laplace pressure, which enhances their ability to retain liquid electrolytes more effectively<sup>115</sup>.

Figures 15d and 15e display the cross-sectional morphology of hot-pressed cellulose-based films. The structures interconnected by the fibers and the interlayer space of films allow electrolytes to penetrate from both transverse and longitudinal directions, leading to a higher electrolyte loading capacity of cellulose-based samples. Figure 15f illustrates the thickness variation of all separators after immersion in the alkaline electrolyte. It can be seen that electrolytes could infiltrate *via* the interlayers of cellulose-based separators, resulting in a significant thickness change in the transverse direction. In contrast, the thickness of the Celgard separator remains virtually unchanged.

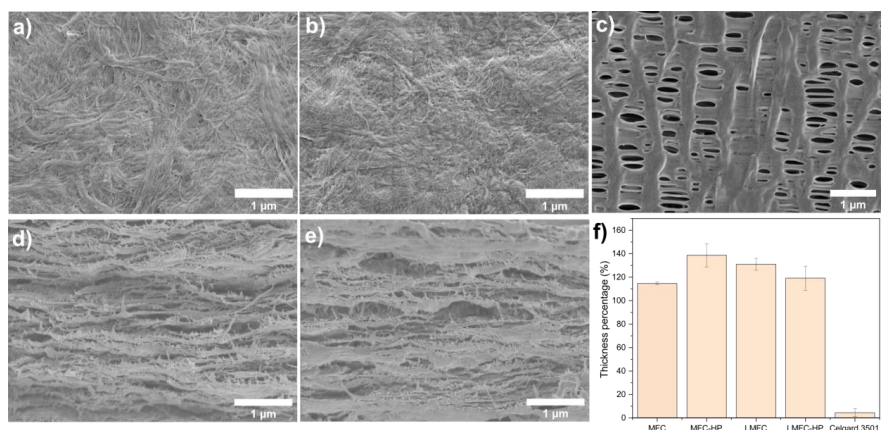


**Figure 15.** SEM images of surfaces of a) MFC-HP, b) LMFC-HP, and c) Celgard 3501; cross-section morphology of d) MFC-HP and e) LMFC-HP; f) thickness changes of all separators after soaking electrolyte (Figures adapted from Paper III).

The thermal properties of separators are critical for ensuring battery safety, particularly in high-power applications. Figure 16 illustrates the thermal behavior of the separators when subjected to elevated temperatures. Upon heating to 150 °C for 30 minutes, commercial Celgard 3501 exhibited significant thermal shrinkage, as shown in Figure 16. At 180 °C, Celgard 3501 completely melted, whereas the MFC and LMFC separators maintained excellent dimensional stability even at elevated temperatures. The inferior thermal stability of commercial Celgard under heating has also been reported by Liu et al<sup>84</sup>. This marked difference in thermal performance highlights a significant limitation of polyolefin-based separators like Celgard 3501, especially for use in high-power electronic devices or electric vehicle batteries, which require stable operation under extreme conditions. The pronounced thermal shrinkage and melting of Celgard at higher temperatures could lead to direct contact between the cathode and anode, particularly during high current operation or overheating, potentially causing short circuits and severe safety hazards.

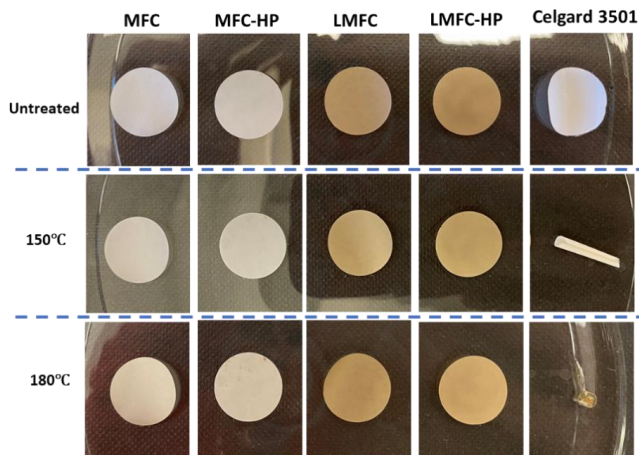


**Figure 16.** Digital photos of separators after heating under different temperatures in an oven (Figures adapted from Paper III).

To evaluate the practical performance of cellulose-based separators in aqueous batteries, symmetrical cells were assembled using MFC, LMFC, MFC-HP, and LMFC-HP films as separators, and their electrochemical properties were compared to commercial Celgard. Figures 17a-17c present the long-term cycling stability of these separators in half cells. Notably, cells with hot-pressed MFC and LMFC separators demonstrated excellent cycling stability over 200 hours, comparable to that of commercial Celgard. EIS measurements of Zinc/separator/Zinc cells were conducted to investigate their interfacial resistance, with results shown in Figure 17d. The diameter of the semicircle in the high-frequency region indicates the charge transfer resistance, with larger diameters corresponding to higher resistance. Cells utilizing cellulose-based separators exhibited lower resistance compared to those with Celgard 3501, indicating the superior electronic transport properties of cells assembled with cellulose-based separators. Interestingly, despite the higher resistance observed in hot-pressed MFC-HP and LMFC-HP separators, these cells displayed improved cycling stability relative to the untreated counterparts. This enhancement is likely due to the superior wet mechanical properties of the hot-pressed separators, which are crucial for maintaining structural integrity during extended cycling in aqueous environments. Moreover, cells assembled with hot-pressed MFC and LMFC separators exhibited lower overpotentials. Overpotential represents the extra voltage required beyond the theoretical value to drive an electrochemical reaction, and it was reduced in cells with cellulose-based separators, signifying their more efficient electrochemical reactions and

improved kinetics within the cells. This suggests that hot-pressed MFC and LMFC separators enhance mechanical stability and contribute to more efficient electrochemical performance.

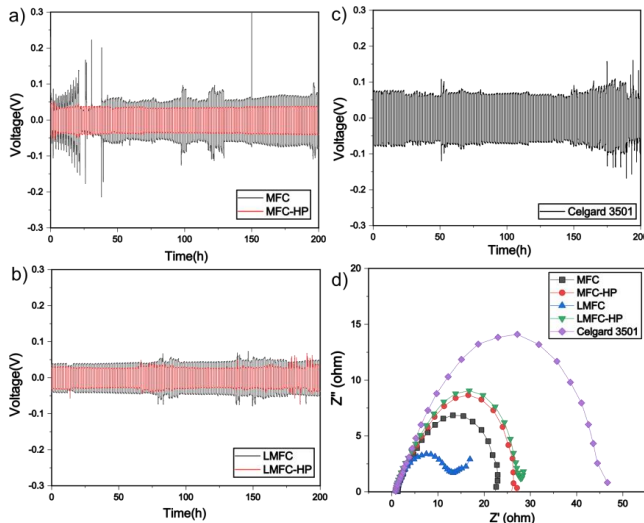


**Figure 17.** Cycling performances of zinc cells with a) MFC and MFC-HP, b) LMFC and LMFC-HP, and c) Celgard 3501 separators. d) EIS measurement of Zinc/separator/Zinc cells using different separators (Figures adapted from Paper III).

### Proton-exchange membranes

A proton exchange membrane (PEM), also known as a polymer electrolyte membrane, is a semipermeable membrane designed to conduct protons while acting as an insulator for electrons and blocking gases such as oxygen and hydrogen<sup>116</sup>. PEMs are a key component in fuel cells, which represent one of the most promising sources of green energy for road transportation, converting chemical energy into electricity with efficiencies reaching up to 80%<sup>117</sup>.

However, the high cost of benchmark synthetic perfluorinated PEMs (e.g., Nafion) (600-1200 US\$ per m<sup>2</sup>) is hindering the wide spread of fuel cells<sup>118</sup>. Additionally, Nafion experiences reduced proton conductivity at elevated temperatures, which limits its performance in high-temperature fuel cell applications<sup>117,119</sup>. This has triggered the exploration of novel, cost-efficient, and sustainable PEMs designed for FCs and electrolysis.

This work investigates the potential of bio-based materials, lignin-containing microfibrillated cellulose, to overcome the environmental and cost-related

drawbacks of synthetic PEMs. The gas transport property and selectivity of LMFCs derived from softwood and hardwood are compared with lignin-free membranes. The impact of relative humidity and operating temperatures on their proton conductivity for practical usage was explored.

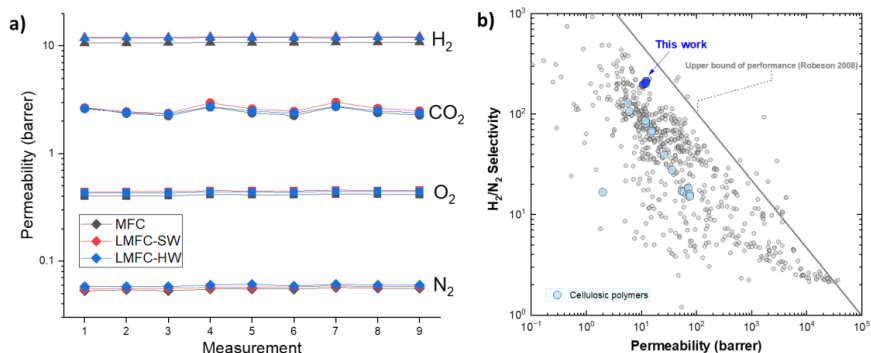


**Figure 18.** a) Small gas permeability of MFC, LMFC-SW, and LMFC-HW membranes measured at 35 °C and a transmembrane pressure of 300 kPa; b) Robeson upper bound plot for the H<sub>2</sub>/N<sub>2</sub> pair (Figure adapted from Paper V).

Figure 18a depicts the gas permeability of produced MFC and LMFC membranes derived from different wood species at a similar thickness between 17.3-18.7  $\mu\text{m}$ . The result shows that the gas transport property of membranes is inversely proportional to the gases' kinetic diameters, and the cellulose-based membranes showed similar gas permeability following selectivity for relevant gas pairs: H<sub>2</sub>/N<sub>2</sub>  $\sim$  210, CO<sub>2</sub>/N<sub>2</sub>  $\sim$  45 and O<sub>2</sub>/N<sub>2</sub>  $\sim$  7.5. The gas transport through these membranes is likely mainly driven by the packing of the cellulose fibers within membranes. As can be seen from the figures, the membranes exhibited excellent gas selectivity, particularly for gas pairs H<sub>2</sub>/N<sub>2</sub> and H<sub>2</sub>/O<sub>2</sub>. The Robeson upper bound plot for gas permeability of the H<sub>2</sub>/N<sub>2</sub> gas pair, depicted in Figure 18b, demonstrates that the membranes studied exhibit the highest selectivity (H<sub>2</sub>/N<sub>2</sub> pair) with proximity to the upper bound among structurally similar cellulosic polymers (represented by light blue points).

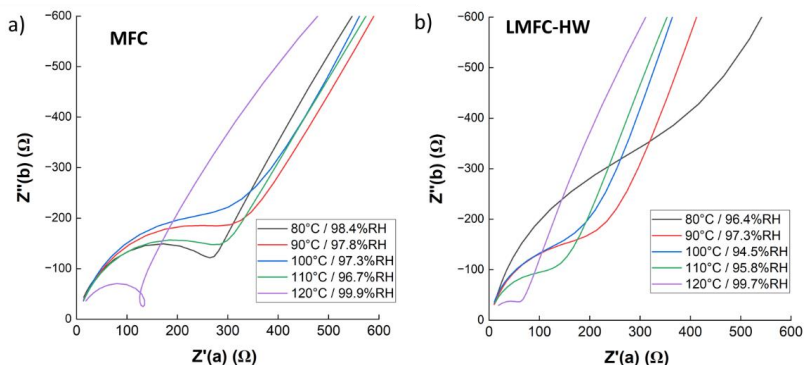


**Figure 19.** Nyquist plots of a) MFC and b) LMFC-HW membranes at different temperatures from 80 to 120 °C with a relative humidity > 95% (Figure adapted from Paper V).

The dependence of the proton conductivity on temperature and relative humidity for the produced lignin-free and lignin-rich membranes is shown in Figures 19 and 20. Figure 19 presents the Nyquist plots for MFC and LMFC-HW membranes at varying temperatures (80-120°C) at highly saturated conditions (> 95%). Notably, in the high-frequency region, the LMFC-HW membranes exhibit significantly lower resistance compared to the MFC membranes. Furthermore, as the temperature increases, the impedance of both MFC and LMFC-HW membranes continuously decreases. The benchmark synthetic perfluorinated PEMs (e.g., Nafion) generally exhibit limited operation at elevated temperatures. As temperature increases, the Nafion membrane loses water more rapidly, reducing its proton transport capacity<sup>120,121</sup>. The cellulose-based membranes showed their potential to be used over a broader range of temperatures.

The change in relative humidity would significantly affect the proton conductivity of the produced membranes, as depicted in Figure 20. All cellulose-based membranes showed low proton conductivity in dry conditions, and it increased about 4 orders of magnitude in humidified conditions. Furthermore, Lignin-rich MFC membranes showed two times higher proton conductivity than lignin-free samples at varied temperatures, as shown in Figure 20b. This is likely caused by the presence of more active proton-donating functional groups, such as carboxylic groups, in the structures of LMFC samples than lignin-free counterparts.

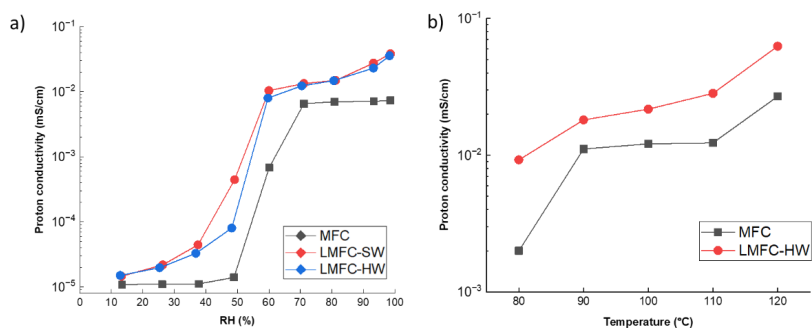


**Figure 20.** a) The proton conductivity of MFC and LMFC membranes at varied relative humidity at 80 °C and (b) dependence of proton conductivity on temperature at saturated humidity (>95%) (Figure adapted from Paper V).

### Membrane for organic dye adsorption

Water pollution caused by industrial dyes is a significant environmental issue. These pollutants often enter water bodies, threatening diverse aquatic and terrestrial organisms. It is estimated that approximately 100 tons of dyes are discharged into water streams annually<sup>122</sup>. These dyes, along with their byproducts, are often toxic and non-biodegradable<sup>123</sup>.

Recently, cellulose nanoparticles have emerged as promising renewable materials for wastewater treatment due to their high surface area, biodegradability, good affinity to dyes and metal ions, and excellent mechanical properties<sup>53</sup>. So far, many commercial adsorbents have been derived from different sources in either powder or granular form. However, a significant drawback of these adsorbents is that most of them require effective pretreatment for dye adsorption<sup>124</sup>. In contrast, membrane-based adsorbents represent an innovative option that combines the advantageous properties of both membranes and traditional adsorbents to remove various water pollutants effectively. Regenerating the surface of membrane-based adsorbents is simpler than materials in powder or granular forms<sup>124,125</sup>. Georgouvelas et al. produced an all-cellulose functional membrane composed of cellulose nanocrystals, TEMPO-oxidized cellulose nanofibers, or zwitterionic polymer grafted cellulose nanocrystals in combination with cellulose fibers and microfibrillated cellulose via a facile, one-step method<sup>122</sup>. The prepared cellulose membranes exhibited superior adsorption capacity as catalysts for water treatment while maintaining excellent water permeability. Another approach for the removal of dyes was the preparation of composite cellulose membranes. Liu et al. developed a method to

prepare double-layered GO (graphene oxide)-CNF membranes with ultrathin GO layer on CNF membrane composed of commercial-grade CNF (Exilva), and the composite membrane showed superior separation of dye molecules *via* cross-flow filtration<sup>126</sup>.

In the present work, "composite" membranes composed of wood-based polymers, cellulose, hemicellulose, and lignin are prepared, and their usage as sustainable adsorbents for synthetic organic dyes, such as MB and CV, were investigated.

### **Effect of lignin on the adsorption properties**

Adsorption capacity is a critical parameter when evaluating materials for use as industrial-scale adsorbents. Given the anionic nature of the cellulose membrane surface, the adsorption performance of the prepared membranes was assessed using two cationic dyes: methylene blue (MB) and crystal violet (CV). As illustrated in Figure 21, LMFC-HW exhibited the highest adsorption capacities, with values of  $99 \pm 3 \mu\text{mol g}^{-1}$  for CV and  $102 \pm 4 \mu\text{mol g}^{-1}$  for MB, achieving removal efficiencies of 40.8% and 42.1%, respectively. In contrast, MFC-SW displayed the lowest adsorption capacities, with  $12 \pm 1 \mu\text{mol g}^{-1}$  for CV and  $17 \pm 2 \mu\text{mol g}^{-1}$  for MB, corresponding to removal efficiencies of 12.3% and 20.6%. The LMFC-SW membrane demonstrated a slightly higher affinity for CV compared to MB, with adsorption capacities of  $85 \pm 3 \mu\text{mol g}^{-1}$  and  $79 \pm 4 \mu\text{mol g}^{-1}$ , and removal efficiencies of 34.4% and 32.0%, respectively. These results suggest that lignin-rich membranes are more promising candidates for adsorbing cationic organic contaminants than their lignin-free counterparts.

The adsorption kinetics of three samples were further investigated. For MB adsorption, 50% removal was achieved within 9 minutes for MFC-SW, 15 minutes for LMFC-SW, and 22 minutes for LMFC-HW. In contrast, 50% CV removal required 31, 25, and 30 minutes for the respective membranes. Notably, 90% removal efficiencies for MB and CV were attained within 16 and 117 minutes for MFC-SW, 72 and 90 minutes for LMFC-SW, and 72 and 120 minutes for LMFC-HW. It revealed that all membranes exhibited faster adsorption rates for MB than for CV. This difference is attributed to the greater mobility and faster diffusion of MB, which possesses a more linear structure and smaller molecular size<sup>127</sup>. Given that the dye concentrations correspond to the plateau regions of the equilibrium isotherms, the rapid adsorption kinetics observed for the lignin-containing membranes underscore their potential for practical applications in efficiently removing cationic contaminants.

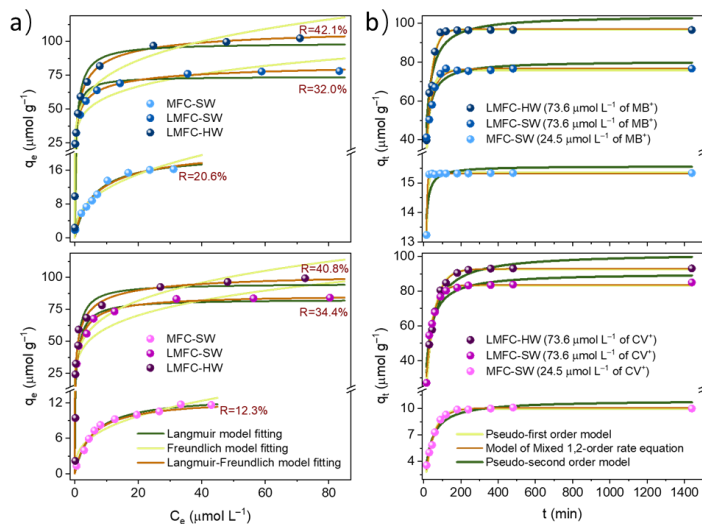


**Figure 21.** a) Adsorption isotherms (shown in symbols) and non-linear fitting by the equilibrium models (shown in lines) of MB (top figure) and CV (bottom figure); (b) influence of contact time and non-linear fitting by the kinetic models (lines) of MB (top figure) and CV (bottom figure) adsorption (symbols) (Figures adapted from Paper IV).

### Effect of pH and ionic strength on adsorption performance

The pH of a solution is a crucial parameter in the adsorption process as it influences both the surface characteristics of the adsorbent and the state of the adsorbate species<sup>128</sup>. Different water sources exhibit varying pH levels depending on their origins. The effect of pH on dye adsorption was evaluated within the range from 5 to 7, with results presented in Figures 22a and 22b. Overall, the use of a buffer solution had a negative impact on adsorption efficiency. MFC-SW membrane was the most sensitive to buffer components, exhibiting a significant decrease in removal efficiency from 31.2% to 9.34% for MB and from 20.3% to 7.12% for CV at pH 7. Adsorption of both dyes was completely inhibited at a pH of 5. In contrast, lignin-rich membranes demonstrated greater resilience to buffer-induced changes.

A minor decline in removal efficiency was noticed with further acidification. For LMFC-SW, adsorption efficiency dropped from 49.8% to 34.2% for MB and from 49.3% to 34.9% for CV. Similarly, LMFC-HW exhibited a decrease from 44.3% to 31.2% for MB and from 49.1% to 39.6% for CV. These results suggest that LMFC-SW and LMFC-HW membranes are likely to perform

better in real wastewater systems containing organic and inorganic contaminants compared to lignin-free membranes.

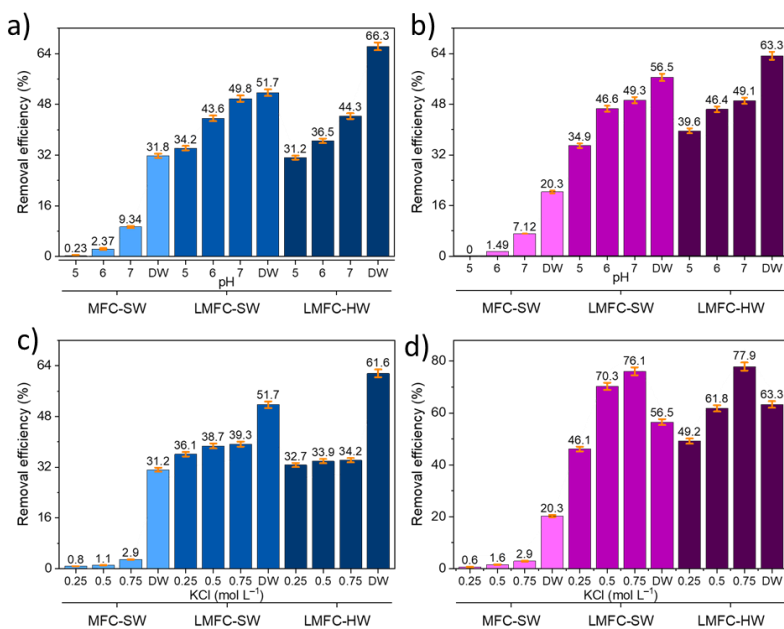


**Figure 22.** The influence of pH on the adsorption of a) MB and b) CV. The influence of ionic strength on the adsorption of c) MB and d) CV (Figures adapted from Paper IV).

Water resources often contain dissolved inorganic species that can interfere with the adsorption behavior of adsorbents. To investigate the impact of ionic strength on adsorption capacity, potassium chloride (KCl) was introduced, and the results are depicted in Figures 22c and 22d. Similar to the impact of pH, MFC-SW was the most sensitive to added ions. The removal efficiency of MFC-SW for dyes dropped dramatically to 0.5–2.9% in the presence of KCl, compared to 31.2% for MB and 20.3% for CV in distilled water. Although KCl also reduces the removal efficiency of lignin-rich membranes for MB adsorption, the decrease was minimal, and the R values remained within the range of uncertainties as the salt concentration varied from 0.25 to 0.75 mol L<sup>-1</sup>. This suggests that the performance of lignin-rich membranes is less susceptible to interference from inorganic components. Overall, both lignin-rich membranes demonstrated effective dye removal even in the presence of

inorganic species, highlighting their potential for practical water treatment applications.

### Dye adsorption from simulated and actual natural wastewater samples

The practical applicability of the membranes as adsorbents was further evaluated on a simulated groundwater sample (SGW) and an actual water sample from the Fyris River in Uppsala, Sweden (ARW). The adsorption spectra of the samples before and after adsorption are showcased in Figure 23. The results indicate that LMFC-SW exhibited the highest water purification performance, achieving removal efficiencies of 83.0% for SGW and 77.6% for ARW, while the LMFC-HW membrane exhibited slightly lower removal efficiencies of 73.5% and 77.3% for SGW and ARW, respectively. However, the MFC-SW membrane showed the lowest effectiveness, with removal efficiencies of 7.4% for SGW and 43.9% for ARW. The reduced performance in SGW can be attributed to the adverse effects of electrolytes on the MFC-SW, similar to the trend shown in Figure 22. These findings further underscore the potential of lignin-rich membranes for practical water purification applications.

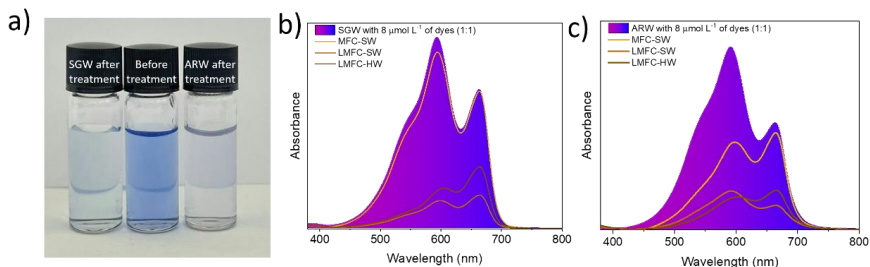


**Figure 23.** a) The water sample containing 8  $\mu\text{mol L}^{-1}$  of dyes MB and CV in a molar ratio of 1:1 (middle bottle), SGW (left bottle), and ARW (right bottle) after treatment with LMFC-SW; b) absorption spectra of SGW with 8  $\mu\text{mol L}^{-1}$  of dyes before and after treating with membranes; c) absorption spectra of ARW with 8  $\mu\text{mol L}^{-1}$  of dyes before and after treating with membranes (Figures adapted from Paper IV).

### 3.6 Recyclability

The recyclability of LMFC films was evaluated by redispersing the once-dried LMFC films in distilled water. As displayed in Figure 24a, the recycled LMFC-SW and LMFC-HW samples exhibited tensile strength of 206 MPa and 148 MPa, respectively.

The inherent compatibility between lignin and cellulose did not compromise the recyclability of the cellulose-based materials. Figures 24b and 24c show that once-dried lignin-rich cellulose films can be well dispersed and reshaped into uniform films. The tensile strength recovery for the LMFC-SW and LMFC-HW films was 71.5% and 63.2%, respectively, surpassing the tensile strength recovery reported for MFC films, which was 50.5% after drying at 100 °C<sup>129</sup>. Hornification, a well-known process that occurs during the drying of cellulose fibers, results from the close proximity of cellulose chains, leading to the formation of intermolecular bonds and irreversible fiber aggregation<sup>129,130</sup>. This process typically co-crystallizes cellulose fibers and diminishes water absorption capacity, thereby limiting fiber swelling of cellulose fibers when re-exposed to a watery environment<sup>131</sup>. Notably, LMFC films exhibited a higher recovery of mechanical properties than MFC films, likely due to the presence of residual lignin, which mitigates the effects of hornification. It can also be noticed that dried LMFC films showed a higher water uptake than MFC films (Figure S3 from paper III), indicating their better swelling ability after drying.

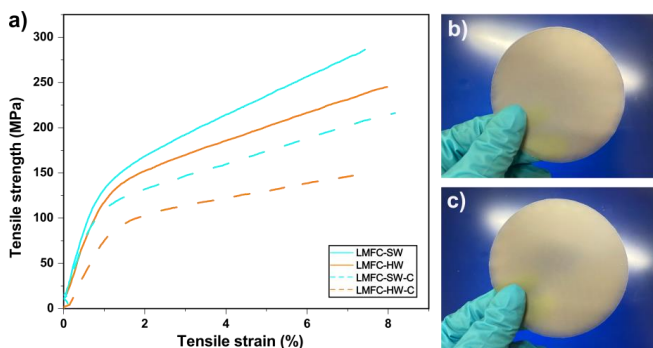


**Figure 24.** a) Typical stress-strain curves of recycled LMFC-SW and LMFC-HW films; Digital images of b) LMFC-SW and c) LMFC-HW films after recycling (Figure adapted from Paper II)<sup>87</sup>.

It is believed that hemicellulose and hemicellulose-lignin matrix could help maintain the contact between fibers, mitigating the occurrence of hornification<sup>132</sup>. The high recovery of tensile properties in LMFC films is crucial for commercializing and transporting nanocellulose products. Since MFC materials often require drying for transportation and subsequent redispersion, the superior recovery of mechanical properties in LMFC films positions them as more promising candidates for commercial use. The recyclability of these films also maximizes resource efficiency, as the reuse of cellulose films reduces the

need for virgin raw materials. Recyclable cellulose films can be reprocessed and repurposed, maintaining their economic value and contributing to sustainable production practices requiring less energy and fewer resources than manufacturing new products from raw materials.



## 4 Summary of the thesis

- i. In the first work, self-standing films composed of lignin-rich microfibrillated cellulose fibers were successfully prepared from high kappa number kraft pulp using a chemical-free method. The presence of residual lignin contributes to improved thermal properties ( $T_{\max} > 345$  °C) and hydrophobicity of produced microfibrillated cellulose films. Their mechanical properties can be further improved at elevated drying temperatures, reaching 283 MPa in tensile strength and 15 GPa in their modulus.
- ii. The impact of raw pulp fibers on the production and properties of produced lignin-rich microfibrillated cellulose films was further investigated. Specifically, hardwood pulps showed a higher degree of defibrillation under the same energy input compared to the softwood counterparts. The failure mechanism of the produced lignin-rich MFC films derived from different wood species was compared, and the result shows that softwood-derived lignin-rich films displayed fewer strain-concentrated regions than hardwood films due to the increased physical fiber bonding formed by their longer fibers, resulting in an enhanced stress transfer through the fiber networks and higher tensile strength. The deviation of their fracture position from the strain-concentrated areas suggests that the failure mode of LMFC-SW films is likely governed by the fiber fracture. The synergistic effect of the more condensed lignin structures in softwood fibers and their longer fibers contributes to the higher stiffness of corresponding softwood-derived lignin-rich films.
- iii. The produced lignin-rich MFC films showed exceptional potential for use in energy storage systems. The wet tensile strength of the produced lignin-rich MFC films was significantly improved after hot-

press treatments, making them more robust in aqueous environments and ideal candidates as separators for aqueous zinc batteries. Additionally, these lignin-rich films exhibit better electrolyte uptake and wettability compared to commercial Celgard 3501, thanks to the inherent hydrophilicity and swelling ability of cellulose fibers and the interlayer structures for electrolyte storage. The lignin-rich cellulose separators showed superior dimensional stability at elevated temperatures and good ionic conductivity. The zinc cells assembled with hot-pressed lignin-rich cellulose separators displayed comparable cycling stability after 200 hours compared to commercial Celgard separators.

- iv. The gas transport properties and proton conductivity of the produced lignin-rich microfibrillated cellulose films were further explored as proton exchange membranes. The gas transport properties revealed that the influence of wood species on gas permeability was insignificant, with their gas barrier properties being primarily governed by fiber packing. The membranes exhibited excellent gas barrier and selectivity, particularly for gas pairs  $H_2/N_2$  and  $H_2/O_2$ , showcasing their potential use in applications requiring high gas barrier performance. Moreover, LMFC membranes demonstrated significantly improved proton conductivity under humidified conditions, with a four-order-of-magnitude increase in conductivity compared to dry conditions. Notably, the LMFC membranes exhibited nearly twice the proton conductivity of the lignin-free counterparts at temperatures up to  $120^\circ C$ , indicating their suitability for use in both hydrated and high-temperature environments.
- v. Lastly, the higher fiber charge in LMFCs and the robust structures of lignin-rich microfibrillated cellulose films make them appealing for cationic organic dye adsorption. The effect of pH and ionic strength on these films was also investigated. Results demonstrated that the presence of lignin significantly increased the dye adsorption capacity of LMFC films in both simulated groundwater and actual river samples. Specifically, LMFC-HW membranes showed an adsorption capacity of  $99 \pm 3 \mu mol g^{-1}$  for CV and  $102 \pm 4 \mu mol g^{-1}$  for MB, while softwood-derived LMFC films demonstrated a capacity of  $85 \pm 3 \mu mol g^{-1}$  for CV and  $79 \pm 4 \mu mol g^{-1}$  for MB, both of which are much higher than MFC-SW counterparts ( $12 \pm 1 \mu mol g^{-1}$  for CV and  $17 \pm 2 \mu mol g^{-1}$  for MB). This good affinity to organic dyes of LMFC

films, combined with their environmentally friendly nature, positions them as viable and sustainable adsorbents for addressing water pollution.



## 5 Conclusions

Material development:

1. Lignin-rich microfibrillated cellulose (LMFC) films, produced from high-kappa number kraft pulp, demonstrate superior thermal stability and mechanical properties compared to lignin-free films, with significant improvements in their mechanical strength achieved by simply adjusting the drying conditions.
2. The structure-property relationships between raw fibers and LMFC films were thoroughly examined. Results reveal that softwood-derived LMFC films exhibit higher tensile strength and stiffness than the hardwood counterparts due to the longer fibers and more condensed lignin structures, which improve stress transfer within the structures.

Applications:

3. LMFC films, particularly after hot-press treatments, show great promise as environmentally friendly separators for aqueous zinc-ion batteries, offering excellent wet strength, electrolyte uptake, wettability, and cycling stability.
4. These LMFC films also exhibit excellent gas transport selectivity and significantly increased proton conductivity in hydrated and high-temperature environments, making them suitable candidates for proton-exchange membranes in energy applications.
5. The potential of LMFC films as sustainable adsorbents for cationic organic dyes is also highlighted, with better adsorption capacities in both simulated groundwater and actual river samples showcased than lignin-free films, positioning them as effective and eco-friendly solutions for addressing water pollution.

This research attempts to deepen our understanding of how raw materials and processing methods can be optimized to produce lignin-containing nano/microcellulose films with desirable properties. Lignin-rich microfibrillated cellulose fibers produced from low-cost and high-yield high-kappa number kraft pulps, offer a scalable and environmentally sustainable alternative. This suggests the potential of LMFC as a cost-effective and eco-friendly material with robust mechanical characteristics suitable for various industrial applications.

## 6 Future outlook

This thesis highlights the potential of lignin-rich microfibrillated cellulose fibers as a sustainable, cost-effective alternative to traditional nanocellulose materials, with promising applications across diverse fields. Compared to TOCNF, LMFC can be prepared using a scalable and environmentally friendly method from low-cost unbleached pulps, and they showed comparable mechanical properties to TOCNF films and excellent thermal stability, demonstrating that it is not always necessary to produce nano-sized cellulose to achieve superior properties. However, several prospects remain for further exploration and improvement, which could significantly enhance the performance and industrial utility of LMFC-based materials.

While this thesis has demonstrated the effectiveness of LMFC films produced from high-kappa number kraft pulps, there is still significant potential for optimizing both raw material selection and processing conditions. Future work could explore using different raw materials, such as pulp obtained from different processes and with different kappa numbers, and the defibrillation techniques to fine-tune lignin content and fiber morphology. Detailed studies on the correlation between lignin content, fiber morphology, and the resulting properties of the membranes could lead to their improved performance in high-temperature and high-humidity applications. Additionally, combining LMFC with other bio-based polymers or fillers may result in hybrid materials with tailored properties for specific end-use applications.

Further investigation can also be conducted to conduct a comparative analysis of films from the same raw material with selective delignification to remove lignin while preserving the fiber length. This can serve as an ideal way to isolate the impact of lignin content/structure further from fiber length effects for a more detailed discussion.

The promising performance of LMFC membranes as separators in aqueous zinc-ion batteries suggests great potential for these materials in the broader field of energy storage. Further research should explore their integration into full cells with commercialized electrode materials. Further functionality of these lignin-rich cellulose membranes using green chemical methods and fine-tuning their structures could also lead to better performances for wastewater treatment and better proton conductivity as proton-exchange membranes.

As LMFC materials are derived from renewable resources, they readily contribute to the circular bio-economy. Future work should include comprehensive life cycle assessments (LCAs) to quantify the environmental impact of LMFC production, usage, and disposal. Exploring the potential for recycling and reprocessing LMFC materials could further enhance their sustainability and reduce reliance on non-renewable, fossil-based materials.

## 7 Acknowledgments

I would like to express my heartfelt gratitude to my supervisors, Assoc. Prof. Olena Sevastyanova, Prof. Artem Kulachenko, and Prof. Monica Ek, for their constant guidance, support, and motivation throughout my PhD journey. Olena, thank you for the great opportunity to involve me in this project and thank you for always encouraging me to think critically and independently, and for your patience in helping me with the challenges of this research. Artem, I am sincerely grateful for your optimism and constructive feedback, which have been a constant source of inspiration. Your door was always open, and your support, both scientific and personal, has been invaluable. Thank you for sharing your insights and for believing in my potential. Monica, I am deeply thankful for all your valuable comments and discussions. Your support has been instrumental, and I am fortunate to have shared this journey with you.

I would like to thank Prof. Mikael E. Lindström for being on the supervision team at the beginning of my PhD journey. Thank you for all your help in shaping this project and discussing new ideas and technical challenges. I am deeply grateful to Prof. Åsa Emmer for her warm support whenever I am in need. I would also like to extend my gratitude to my collaborators and co-authors who contributed to our collaborative work and my research progress. I am especially thankful to Dr. Bin Chen, Dr. Roman, and Dr. Sadegh for their invaluable help with the experimental work and for sharing their expertise. Dr. Raquel Bohn Stoltz is also acknowledged for the valuable discussions.

I also want to especially acknowledge Dr. Cláudia Esteves, Dr. Lengwan Li, and Dr. Erfan Oliaei for all the discussions and their invaluable help. Thank you to all the colleagues and friends, Isabella, Fika, Maria, Pär, Jenny, Antonia, Vijaya, Eashwara, Taoran, Carl, Raghu, Ioanna, Jonas, Maria F., Iuliana, Johanna, Jowan, Marie, Mu-Rong, Antonio, Nazmun, Dimitrios, Jyoti, and

Georgios, for all your help and making this time enjoyable and memorable. I would like to thank Prof. Lars, Dr. Per, Assoc. Prof. Yuanyuan, Dr. Tomas, Dr. Anastasia, Prof. Martin, and Prof. Gunnar for the scientific discussions and invaluable knowledge.

To my friends, thank you for making life outside of the lab just as fulfilling. Your companionship has been a constant source of joy, and I am deeply grateful for all the moments of laughter, sports, and adventures we've shared.

This work would not have been possible without the financial support of The China Scholarship Council, Karl Engvers Stiftelse, and the Wood and Pulping Chemistry Research Network (WPCRN). I am deeply grateful for their financial support for this research. Valmet is also acknowledged for providing raw materials for this project.

Finally, I want to express my deepest appreciation to my family. To my sister, thank you for always being there to encourage me and share my thoughts and for your faith in my abilities. To my parents, words cannot express how grateful I am for your endless love, support, and encouragement. I love you! 谢谢你们!  
我爱你们!

Thank you all for making this journey possible.

Stockholm, October 2024,

Huisi Li

李慧思

## 8 References

1. Li Q, McGinnis S, Sydnor C, Wong A, Renneckar S. Nanocellulose life cycle assessment. *ACS Sustain Chem Eng.* 2013;1(8):919-928. doi:10.1021/sc4000225
2. Arvidsson R, Nguyen D, Svanström M. Life cycle assessment of cellulose nanofibrils production by mechanical treatment and two different pretreatment processes. *Environ Sci Technol.* 2015;49(11):6881-6890. doi:10.1021/acs.est.5b00888
3. Isikgor FH, Becer CR. Lignocellulosic biomass: a sustainable platform for the production of bio-based chemicals and polymers. *Polym Chem.* 2015;6(25):4497-4559. doi:10.1039/c5py00263j
4. Nechyporchuk O, Belgacem MN, Bras J. Production of cellulose nanofibrils: A review of recent advances. *Ind Crops Prod.* 2016;93:2-25. doi:10.1016/j.indcrop.2016.02.016
5. Liu K, Du H, Zheng T, et al. Lignin-containing cellulose nanomaterials: Preparation and applications. *Green Chem.* 2021;23(24):9723-9746. doi:10.1039/d1gc02841c
6. Solala I, Iglesias MC, Peresin MS. On the potential of lignin-containing cellulose nanofibrils (LCNFs): a review on properties and applications. *Cellulose.* 2020;27(4):1853-1877. doi:10.1007/s10570-019-02899-8
7. Chen C, Hu L. Nanoscale Ion Regulation in Wood-Based Structures and Their Device Applications. *Adv Mater.* 2021;33(28):1-28. doi:10.1002/adma.202002890
8. Sjöström E. the Structure of Wood. *Wood Chem.* Published online 1993:1-20. doi:10.1016/b978-0-08-092589-9.50005-x
9. Brown RM, Saxena IM, Kudlicka K. Cellulose biosynthesis in higher plants. *Trends Plant Sci.* 1996;1(5):149-156.
10. Ek M, Gellerstedt G, Henriksson G. *Wood Chemistry and Wood Biotechnology.* Walter de Gruyter; 2009.
11. Sjöstrom E. *Wood Chemistry: Fundamentals and Applications.* Elsevier; 2013.
12. N.J. Heyn A. The elementary fibril and supermolecular structure of cellulose in soft wood fiber. *J Ultrastructure Res.* 1969;26(1-2):52-68. doi:10.1016/S0022-

13. dos Santos Abreu H, Professor A, Ant M, Maria nio. LIGNIN STRUCTURE AND WOOD PROPERTIES Alexandre Miguel do Nascimento. *Wood Fiber Sci.* 1999;31(4):426-433. <https://wfs.swst.org/index.php/wfs/article/view/1808>
14. Adler E. Lignin chemistry—past, present and future. *Wood Sci Technol.* 1977;11(3):169-218.
15. Ralph J, Lundquist K, Brunow G, et al. Lignins: Natural polymers from oxidative coupling of 4-hydroxyphenyl- propanoids. *Phytochem Rev.* 2004;3(1-2):29-60. doi:10.1023/B:PHYT.0000047809.65444.a4
16. Henriksson G. 6. Lignin. *Wood Chem wood Biotechnol.* Published online 2009:121-146.
17. Freudenberg K, Neish AC. Constitution and biosynthesis of lignin. Published online 1968.
18. Xu C, Arancon RAD, Labidi J, Luque R. Lignin depolymerisation strategies: Towards valuable chemicals and fuels. *Chem Soc Rev.* 2014;43(22):7485-7500. doi:10.1039/c4cs00235k
19. Liu Q, Luo L, Zheng L. Lignins: biosynthesis and biological functions in plants. *Int J Mol Sci.* 2018;19(2):335.
20. Thomas B, Raj MC, Athira BK, et al. Nanocellulose, a Versatile Green Platform: From Biosources to Materials and Their Applications. *Chem Rev.* 2018;118(24):11575-11625. doi:10.1021/acs.chemrev.7b00627
21. Balea A, Merayo N, De La Fuente E, Negro C, Blanco Á. Assessing the influence of refining, bleaching and TEMPO-mediated oxidation on the production of more sustainable cellulose nanofibers and their application as paper additives. *Ind Crops Prod.* 2017;97:374-387. doi:10.1016/J.INDCROP.2016.12.050
22. Kurihara T, Isogai A. Properties of poly (acrylamide)/TEMPO-oxidized cellulose nanofibril composite films. *Cellulose.* 2014;21(1):291-299.
23. Ahankari SS, Subhedar AR, Bhadauria SS, Dufresne A. Nanocellulose in food packaging: A review. *Carbohydr Polym.* 2021;255(December 2020):117479. doi:10.1016/j.carbpol.2020.117479
24. Huang C, Dong H, Zhang Z, Bian H, Yong Q. Procuring the nano-scale lignin in prehydrolyzate as ingredient to prepare cellulose nanofibril composite film with multiple functions. *Cellulose.* 2020;27(16):9355-9370. doi:10.1007/s10570-020-03427-9
25. Zhang C wei, Nair SS, Chen H, Yan N, Farnood R, Li F yi. Thermally stable, enhanced water barrier, high strength starch bio-composite reinforced with lignin containing cellulose nanofibrils. *Carbohydr Polym.* 2020;230(July 2019):115626. doi:10.1016/j.carbpol.2019.115626
26. Wang Z, Lee YH, Kim SW, Seo JY, Lee SY, Nyholm L. Why Cellulose-Based Electrochemical Energy Storage Devices? *Adv Mater.* 2021;33(28). doi:10.1002/adma.202000892
27. Parit M, Saha P, Davis VA, Jiang Z. Transparent and Homogenous Cellulose Nanocrystal/Lignin UV-Protection Films. Published online 2018. doi:10.1021/acsomega.8b01345

28. Oliaei E, Lindén PA, Wu Q, Berthold F, Berglund L, Lindström T. Microfibrillated lignocellulose (MFLC) and nanopaper films from unbleached kraft softwood pulp. *Cellulose*. 2020;27(4):2325-2341. doi:10.1007/s10570-019-02934-8
29. Rånby BG. The Colloidal Properties of Cellulose Micelles. *Discuss Faraday Soc*. 1951;11(111):158-164.
30. Wågberg L, Decher G, Norgren M, Lindström T, Ankerfors M, Axnäs K. The build-up of polyelectrolyte multilayers of microfibrillated cellulose and cationic polyelectrolytes. *Langmuir*. 2008;24(3):784-795. doi:10.1021/la702481v
31. Isogai A, Saito T, Fukuzumi H. TEMPO-oxidized cellulose nanofibers. *Nanoscale*. 2011;3(1):71-85. doi:10.1039/c0nr00583e
32. Henriksson M, Henriksson G, Berglund LA, Lindström T. An environmentally friendly method for enzyme-assisted preparation of microfibrillated cellulose (MFC) nanofibers. *Eur Polym J*. 2007;43(8):3434-3441.
33. Nakagaito AN, Yano H. The effect of morphological changes from pulp fiber towards nano-scale fibrillated cellulose on the mechanical properties of high-strength plant fiber based composites. *Appl Phys A Mater Sci Process*. 2004;78(4):547-552. doi:10.1007/s00339-003-2453-5
34. Henriksson M, Henriksson G, Berglund LA, Lindström T. An environmentally friendly method for enzyme-assisted preparation of microfibrillated cellulose (MFC) nanofibers. *Eur Polym J*. 2007;43(8):3434-3441. doi:10.1016/j.eurpolymj.2007.05.038
35. Spence KL, Venditti RA, Habibi Y, Rojas OJ, Pawlak JJ. The effect of chemical composition on microfibrillar cellulose films from wood pulps: Mechanical processing and physical properties. *Bioresour Technol*. 2010;101(15):5961-5968. doi:10.1016/j.biortech.2010.02.104
36. Turbak AF, Snyder FW, Sandberg KR. Microfibrillated cellulose, a new cellulose product: properties, uses, and commercial potential. In: *J Appl Polym Sci Appl Polym Symp*. Vol 37. ; 1983:815-827.
37. Chen Y, Fan D, Han Y, et al. Effect of high residual lignin on the properties of cellulose nanofibrils/films. *Cellulose*. 2018;25(11):6421-6431. doi:10.1007/s10570-018-2006-x
38. Moon RJ, Martini A, Nairn J, Simonsen J, Youngblood J. *Cellulose Nanomaterials Review: Structure, Properties and Nanocomposites*. Vol 40.; 2011. doi:10.1039/c0cs00108b
39. Wang Y, Liu S, Wang Q, Fu X, Fatehi P. Performance of polyvinyl alcohol hydrogel reinforced with lignin-containing cellulose nanocrystals. *Cellulose*. 2020;27(15):8725-8743. doi:10.1007/s10570-020-03396-z
40. Agarwal UP, Ralph SA, Reiner RS, et al. Production of high lignin-containing and lignin-free cellulose nanocrystals from wood. *Cellulose*. 2018;25(10):5791-5805. doi:10.1007/s10570-018-1984-z
41. Ewulonu CM, Liu X, Wu M, Huang Y. Ultrasound-assisted mild sulphuric acid ball milling preparation of lignocellulose nanofibers (LCNFs) from sunflower stalks (SFS). *Cellulose*. 2019;26(7):4371-4389. doi:10.1007/s10570-019-02382-4

42. Shinichiro Iwamoto, Kentaro Abe and HY, Research. The Effect of Hemicelluloses on Wood Pulp Nanofibrillation and Nanofiber Network Characteristics. *Biomacromolecules*. 2007;8(8):2485-2491. doi:10.1021/BM0703970
43. Saito T, Kimura S, Nishiyama Y, Isogai A. Cellulose nanofibers prepared by TEMPO-mediated oxidation of native cellulose. *Biomacromolecules*. 2007;8(8):2485-2491. doi:10.1021/bm0703970
44. Wen Y, Yuan Z, Liu X, et al. Preparation and Characterization of Lignin-Containing Cellulose Nanofibril from Poplar High-Yield Pulp via TEMPO-Mediated Oxidation and Homogenization. *ACS Sustain Chem Eng*. 2019;7(6):6131-6139. doi:10.1021/acssuschemeng.8b06355
45. Zhang N, Tao P, Lu Y, Nie S. Effect of lignin on the thermal stability of cellulose nanofibrils produced from bagasse pulp. *Cellulose*. 2019;26(13-14):7823-7835. doi:10.1007/s10570-019-02657-w
46. Bian H, Chen L, Gleisner R, Dai H, Zhu JY. Producing wood-based nanomaterials by rapid fractionation of wood at 80 °c using a recyclable acid hydrotrope. *Green Chem*. 2017;19(14):3370-3379. doi:10.1039/c7gc00669a
47. Roman M, Winter WT. Effect of sulfate groups from sulfuric acid hydrolysis on the thermal degradation behavior of bacterial cellulose. *Biomacromolecules*. 2004;5(5):1671-1677. doi:10.1021/bm034519+
48. Grishkewich N, Mohammed N, Tang J, Tam KC. Recent advances in the application of cellulose nanocrystals. *Curr Opin Colloid Interface Sci*. 2017;29:32-45. doi:10.1016/j.cocis.2017.01.005
49. Xu T, Du H, Liu H, et al. Advanced Nanocellulose-Based Composites for Flexible Functional Energy Storage Devices. *Adv Mater*. 2021;33(48). doi:10.1002/adma.202101368
50. Henriksson M, Berglund LA, Isaksson P, Lindström T, Nishino T. Cellulose nanopaper structures of high toughness. *Biomacromolecules*. 2008;9(6):1579-1585. doi:10.1021/bm800038n
51. Zhang Y, Wei Y, Qian Y, Zhang M, Zhu P, Chen G. Lignocellulose enabled highly transparent nanopaper with tunable ultraviolet-blocking performance and superior durability. *ACS Sustain Chem Eng*. 2020;8(46):17033-17041. doi:10.1021/acssuschemeng.0c04145
52. Liu W, Liu K, Du H, et al. Cellulose Nanopaper: Fabrication, Functionalization, and Applications. *Nano-Micro Lett*. 2022;14(1):1-27. doi:10.1007/s40820-022-00849-x
53. Kausar A, Zohra ST, Ijaz S, et al. Cellulose-based materials and their adsorptive removal efficiency for dyes: A review. *Int J Biol Macromol*. 2023;224(July 2022):1337-1355. doi:10.1016/j.ijbiomac.2022.10.220
54. Grzybek P, Dudek G, van der Bruggen B. Cellulose-based films and membranes: A comprehensive review on preparation and applications. *Chem Eng J*. 2024;495(June). doi:10.1016/j.cej.2024.153500
55. Peng Y, Gardner DJ, Han Y, Kiziltas A, Cai Z, Tshabalala MA. Influence of drying method on the material properties of nanocellulose I: Thermostability and crystallinity. *Cellulose*. 2013;20(5):2379-2392. doi:10.1007/s10570-013-0019-z

56. Sinquefield S, Ciesielski PN, Li K, Gardner DJ, Ozcan S. Nanocellulose Dewatering and Drying: Current State and Future Perspectives. *ACS Sustain Chem Eng*. 2020;8(26):9601-9615. doi:10.1021/acssuschemeng.0c01797
57. Dufresne A, Cavail`lé JY, Vignon MR. Mechanical behavior of sheets prepared from sugar beet cellulose microfibrils. *J Appl Polym Sci*. 1997;64(6):1185-1194. doi:10.1002/(sici)1097-4628(19970509)64:6<1185::aid-app19>3.3.co;2-2
58. Kurihara T, Isogai A. Properties of poly(acrylamide)/TEMPO-oxidized cellulose nanofibril composite films. doi:10.1007/s10570-013-0124-z
59. Wang X, Sun H, Bai H, Zhang LP. Thermal, Mechanical, and Degradation Properties of Nanocomposites Prepared using Lignin-Cellulose Nanofibers and Poly(Lactic Acid). *BioResources*. 2014;9(2):3211-3224. doi:10.15376/biores.9.2.3211-3224
60. Aulin C, Gällstedt M, Lindström T. Oxygen and oil barrier properties of microfibrillated cellulose films and coatings. *Cellulose*. 2010;17(3):559-574. doi:10.1007/s10570-009-9393-y
61. Fortunati E, Mattioli S, Armentano I, Kenny JM. Spin coated cellulose nanocrystal / silver nanoparticle films. *Carbohydr Polym*. 2014;113:394-402. doi:10.1016/j.carbpol.2014.07.010
62. Zhang X, Li J, Qi K, et al. An Ion-Sieving Janus Separator toward Planar Electrodeposition for Deeply Rechargeable Zn-Metal Anodes. *Adv Mater*. 2022;34(38):1-9. doi:10.1002/adma.202205175
63. Shanmugam K, Varanasi S, Garnier G, Batchelor W. Rapid preparation of smooth nanocellulose films using spray coating. *Cellulose*. 2017;24(7):2669-2676. doi:10.1007/s10570-017-1328-4
64. Bayer T, Cuning BV, Šmíd B, et al. Spray deposition of sulfonated cellulose nanofibers as electrolyte membranes in fuel cells. *Cellulose*. 2021;28(3):1355-1367. doi:10.1007/s10570-020-03593-w
65. Shanmugam K. Methods for Fabrication of Freestanding Nanocellulose Film as a Sustainable Material for Packaging and Biomedical Applications: A Review. *Sci Soc Res*. 2024;6(3):29-40. doi:10.26689/ssr.v6i3.6350
66. Sehaqui H, Morimune S, Nishino T, Berglund LA. Stretchable and strong cellulose nanopaper structures based on polymer-coated nanofiber networks: An alternative to nonwoven porous membranes from electrospinning. *Biomacromolecules*. 2012;13(11):3661-3667. doi:10.1021/bm301105s
67. Pan R, Cheung O, Wang Z, et al. Mesoporous Cladophora cellulose separators for lithium-ion batteries. *J Power Sources*. 2016;321:185-192. doi:10.1016/j.jpowsour.2016.04.115
68. Lee BX, Kjaerulf F, Turner S, et al. Transforming our world: implementing the 2030 agenda through sustainable development goal indicators. *J Public Health Policy*. 2016;37:13-31.
69. Colglazier W. Sustainable development agenda: 2030. *Science (80- )*. 2015;349(6252):1048-1050.
70. Delgado-Aguilar M, Tarrés Q, Pèlach MÀ, Mutjé P, Fullana-I-Palmer P. Are Cellulose Nanofibers a Solution for a More Circular Economy of Paper Products? *Environ Sci Technol*. 2015;49(20):12206-12213. doi:10.1021/acs.est.5b02676

71. Esteves C V., Sevastyanova O, Östlund S, Brännvall E. Differences and similarities between kraft and oxygen delignification of softwood fibers: effects on chemical and physical properties. *Cellulose*. 2021;28(5):3149-3167. doi:10.1007/s10570-021-03713-0
72. Li H, Chen B, Kulachenko A, Jurkijane V, Mathew AP, Sevastyanova O. A comparative study of lignin-containing microfibrillated cellulose fibers produced from softwood and hardwood pulps. *Cellulose*. 2024;31(2):907-926. doi:10.1007/s10570-023-05674-y
73. Ponomarenko J, Dizhbite T, Lauberts M, Volperts A, Dobele G, Telysheva G. Analytical pyrolysis—A tool for revealing of lignin structure-antioxidant activity relationship. *J Anal Appl Pyrolysis*. 2015;113:360-369.
74. Foster EJ, Moon RJ, Agarwal UP, et al. Current characterization methods for cellulose nanomaterials. *Chem Soc Rev*. 2018;47(8):2609-2679. doi:10.1039/c6cs00895j
75. Horvath E. Appropriate conditions for polyelectrolyte titration to determine the charge of cellulosic fibers. Published online 2003.
76. Li H, Kulachenko A, Mathew AP, Stoltz RB, Sevastyanova O. Enhancing the Strength and Flexibility of Microfibrillated Cellulose Films from Lignin-Rich Kraft Pulp. *ACS Sustain Chem Eng*. Published online 2023. doi:10.1021/acssuschemeng.3c05086
77. Katz S, Beatson RP. The determination of strong and weak acidic groups in sulfite pulps. *Sven papperstidning*. 1984;87(6):48-53.
78. Li L, Maddalena L, Nishiyama Y, Carosio F, Ogawa Y, Berglund LA. Recyclable nanocomposites of well-dispersed 2D layered silicates in cellulose nanofibril (CNF) matrix. *Carbohydr Polym*. 2022;279(December 2021):119004. doi:10.1016/j.carbpol.2021.119004
79. Larsson PA, Riazanova A V., Cinar Ciftci G, et al. Towards optimised size distribution in commercial microfibrillated cellulose: a fractionation approach. *Cellulose*. 2019;26(3):1565-1575. doi:10.1007/s10570-018-2214-4
80. Chen B, Coppieters S. Meshfree Digital Image Correlation Using Element Free Galerkin Method: Theory, Algorithm and Validation. *Exp Mech*. 2023;63(3):517-528.
81. Schreier H, Orteu JJ, Sutton MA. *Image Correlation for Shape, Motion and Deformation Measurements: Basic Concepts, Theory and Applications*. Vol 1. Springer; 2009.
82. Cao P, Zhou H, Zhou X, Du Q, Tang J, Yang J. Stabilizing Zinc Anodes by a Cotton Towel Separator for Aqueous Zinc-Ion Batteries. *ACS Sustain Chem Eng*. 2022;10(26):8350-8359. doi:10.1021/acssuschemeng.2c01133
83. Yang Y, Huang C, Gao G, Hu C, Luo L, Xu J. Aramid nanofiber/bacterial cellulose composite separators for lithium-ion batteries. *Carbohydr Polym*. 2020;247(April):116702. doi:10.1016/j.carbpol.2020.116702
84. Liu A, Jiang Z, Li S, et al. A degradable membrane based on lignin-containing cellulose for high-energy lithium-ion batteries. *Int J Biol Macromol*. 2022;213(May):690-698. doi:10.1016/j.ijbiomac.2022.06.004
85. Zhou W, Zhu D, He J, et al. A scalable top-down strategy toward practical metrics

- of Ni-Zn aqueous batteries with total energy densities of 165 W h kg<sup>-1</sup> and 506 W h L<sup>-1</sup>. *Energy Environ Sci.* 2020;13(11):4157-4167. doi:10.1039/d0ee01221a
86. Li H, Kulachenko A, Mathew AP, Stoltz RB, Sevastyanova O. Enhancing the Strength and Flexibility of Microfibrillated Cellulose Films from Lignin-Rich Kraft Pulp. *ACS Sustain Chem Eng.* 2023;11(47):16793-16805. doi:10.1021/acssuschemeng.3c05086
  87. Li H, Chen B, Kulachenko A, Jurkjane V, Mathew AP, Sevastyanova O. A comparative study of lignin-containing microfibrillated cellulose fibers produced from softwood and hardwood pulps. *Cellulose.* 2024;31(2):907-926. doi:10.1007/s10570-023-05674-y
  88. Oliaei E, Berthold F, Berglund LA, Lindström T. Eco-Friendly High-Strength Composites Based on Hot-Pressed Lignocellulose Microfibrils or Fibers. *ACS Sustain Chem Eng.* 2021;9(4):1899-1910. doi:10.1021/acssuschemeng.0c08498
  89. Huang Y, Nair SS, Chen H, Fei B, Yan N, Feng Q. Lignin-Rich Nanocellulose Fibrils Isolated from Parenchyma Cells and Fiber Cells of Western Red Cedar Bark. *ACS Sustain Chem Eng.* 2019;7(18):15607-15616. doi:10.1021/acssuschemeng.9b03634
  90. E2550-21 AI. Standard Test Method for Thermal Stability by Thermogravimetry. *ASTM Int.* 2017;11:5. doi:10.1520/E2550-11.2.
  91. Nair SS, Yan N. Effect of high residual lignin on the thermal stability of nanofibrils and its enhanced mechanical performance in aqueous environments. *Cellulose.* 2015;22(5):3137-3150. doi:10.1007/s10570-015-0737-5
  92. Yang H, Yan R, Chen H, Lee DH, Zheng C. Characteristics of hemicellulose, cellulose and lignin pyrolysis. *Fuel.* 2007;86(12-13):1781-1788. doi:10.1016/j.fuel.2006.12.013
  93. Carvalho DM de, Moser C, Lindström ME, Sevastyanova O. Impact of the chemical composition of cellulosic materials on the nanofibrillation process and nanopaper properties. *Ind Crops Prod.* 2019;127(September 2018):203-211. doi:10.1016/j.indcrop.2018.10.052
  94. Vänskä E, Vihelä T, Peresin MS, Vartiainen J, Hummel M, Vuorinen T. Residual lignin inhibits thermal degradation of cellulosic fiber sheets. *Cellulose.* 2016;23(1):199-212. doi:10.1007/s10570-015-0791-z
  95. Kim HJ, Roy S, Rhim JW. Effects of various types of cellulose nanofibers on the physical properties of the CNF-based films. *J Environ Chem Eng.* 2021;9(5):106043. doi:10.1016/j.jece.2021.106043
  96. Rodríguez-Fabià S, Torstensen J, Johansson L, Syverud K. Hydrophobisation of lignocellulosic materials part I: physical modification. *Cellulose.* 2022;29(10):5375-5393. doi:10.1007/s10570-022-04620-8
  97. Tagami A, Gioia C, Lauberts M, et al. Solvent fractionation of softwood and hardwood kraft lignins for more efficient uses: Compositional, structural, thermal, antioxidant and adsorption properties. *Ind Crops Prod.* 2019;129(December 2018):123-134. doi:10.1016/j.indcrop.2018.11.067
  98. Henriksson G, Germgård U, Lindström ME. A review on chemical mechanisms of kraft pulping. *Nord Pulp Pap Res J.* 2024;(0).

99. Gioia C, Colonna M, Tagami A, et al. Lignin-Based Epoxy Resins: Unravelling the Relationship between Structure and Material Properties. *Biomacromolecules*. 2020;21(5):1920-1928. doi:10.1021/acs.biomac.0c00057
100. Kulachenko A, Denoyelle T, Galland S, Lindström SB. Elastic properties of cellulose nanopaper. *Cellulose*. 2012;19(3):793-807. doi:10.1007/s10570-012-9685-5
101. Salmèn L. Temperature and water induced softening behavior of wood fiber based materials. *Dep Pap Technol*. Published online 1982:150.
102. Salmén L. Viscoelastic properties of in situ lignin under water-saturated conditions. *J Mater Sci*. 1984;19(9):3090-3096. doi:10.1007/BF01026988
103. Mattsson A, Joelsson T, Miettinen A, Ketoja JA, Pettersson G, Engstrand P. Lignin inter-diffusion underlying improved mechanical performance of hot-pressed paper webs. *Polymers (Basel)*. 2021;13(15). doi:10.3390/polym13152485
104. Berglund J, Mikkelsen D, Flanagan BM, et al. Wood hemicelluloses exert distinct biomechanical contributions to cellulose fibrillar networks. *Nat Commun*. 2020;11(1):4692.
105. Terrett OM, Dupree P. Covalent interactions between lignin and hemicelluloses in plant secondary cell walls. *Curr Opin Biotechnol*. 2019;56:97-104.
106. Sevastyanova O, Helander M, Chowdhury S, et al. Tailoring the molecular and thermo-mechanical properties of kraft lignin by ultrafiltration. *J Appl Polym Sci*. 2014;131(18).
107. Abe K, Nakatsubo F, Yano H. High-strength nanocomposite based on fibrillated chemi-thermomechanical pulp. *Compos Sci Technol*. 2009;69(14):2434-2437. doi:10.1016/j.compscitech.2009.06.015
108. Jiang B, Chen C, Liang Z, et al. Lignin as a Wood-Inspired Binder Enabled Strong, Water Stable, and Biodegradable Paper for Plastic Replacement. *Adv Funct Mater*. 2020;30(4):1-11. doi:10.1002/adfm.201906307
109. Kulachenko A, Uesaka T. Direct simulations of fiber network deformation and failure. *Mech Mater*. 2012;51:1-14. doi:10.1016/j.mechmat.2012.03.010
110. Rojo E, Peresin MS, Sampson WW, et al. Comprehensive elucidation of the effect of residual lignin on the physical, barrier, mechanical and surface properties of nanocellulose films. *Green Chem*. 2015;17(3):1853-1866. doi:10.1039/c4gc02398f
111. Tang B, Shan L, Liang S, Zhou J. Issues and opportunities facing aqueous zinc-ion batteries. *Energy Environ Sci*. 2019;12(11):3288-3304. doi:10.1039/c9ee02526j
112. Zampardi G, La Mantia F. Open challenges and good experimental practices in the research field of aqueous Zn-ion batteries. *Nat Commun*. 2022;13(1):1-5. doi:10.1038/s41467-022-28381-x
113. Kumar D, Ail U, Wu Z, et al. Zinc salt in “Water-in-Polymer Salt Electrolyte” for Zinc-Lignin Batteries: Electroactivity of the Lignin Cathode. *Adv Sustain Syst*. 2023;7(4):1-10. doi:10.1002/adsu.202200433
114. Li L, Jia S, Cheng Z, Zhang C. Improved Strategies for Separators in Zinc-Ion Batteries. *ChemSusChem*. 2023;16(8). doi:10.1002/cssc.202202330

115. Ajdary R, Tardy BL, Mattos BD, Bai L, Rojas OJ. Plant Nanomaterials and Inspiration from Nature: Water Interactions and Hierarchically Structured Hydrogels. *Adv Mater.* 2021;33(28). doi:10.1002/adma.202001085
116. Chibac-Scutaru AL, Coseri S. Advances in the use of cellulose-based proton exchange membranes in fuel cell technology: A review. *Int J Biol Macromol.* 2023;247(June):125810. doi:10.1016/j.ijbiomac.2023.125810
117. Selyanchyn O, Selyanchyn R, Lyth SM. A Review of Proton Conductivity in Cellulosic Materials. *Front Energy Res.* 2020;8(November):1-17. doi:10.3389/fenrg.2020.596164
118. Jiang GP, Zhang J, Qiao JL, et al. Bacterial nanocellulose/Nafion composite membranes for low temperature polymer electrolyte fuel cells. *J Power Sources.* 2015;273:697-706. doi:10.1016/j.jpowsour.2014.09.145
119. Selyanchyn O, Bayer T, Klotz D, Selyanchyn R, Sasaki K, Lyth SM. Cellulose Nanocrystals Crosslinked with Sulfosuccinic Acid as Sustainable Proton Exchange Membranes for Electrochemical Energy Applications. *Membranes (Basel).* 2022;12(7). doi:10.3390/membranes12070658
120. Liu L, Chen W, Li Y. An overview of the proton conductivity of nafion membranes through a statistical analysis. *J Memb Sci.* 2016;504:1-9. doi:10.1016/j.memsci.2015.12.065
121. Bayer T, Cuning B V., Selyanchyn R, et al. High temperature proton conduction in nanocellulose membranes: Paper fuel cells. *Chem Mater.* 2016;28(13):4805-4814. doi:10.1021/acs.chemmater.6b01990
122. Georgouvelas D, Abdelhamid HN, Li J, Edlund U, Mathew AP. All-cellulose functional membranes for water treatment: Adsorption of metal ions and catalytic decolorization of dyes. *Carbohydr Polym.* 2021;264(March):118044. doi:10.1016/j.carbpol.2021.118044
123. Dutta S, Gupta B, Srivastava SK, Gupta AK. Recent advances on the removal of dyes from wastewater using various adsorbents: A critical review. *Mater Adv.* 2021;2(14):4497-4531. doi:10.1039/d1ma00354b
124. Dlamini DS, Tesha JM, Vilakati GD, et al. A critical review of selected membrane- and powder-based adsorbents for water treatment: Sustainability and effectiveness. *J Clean Prod.* 2020;277:123497. doi:10.1016/j.jclepro.2020.123497
125. Norfarhana AS, Ilyas RA, Ngadi N. A review of nanocellulose adsorptive membrane as multifunctional wastewater treatment. *Carbohydr Polym.* 2022;291(February):119563. doi:10.1016/j.carbpol.2022.119563
126. Liu P, Zhu C, Mathew AP. Mechanically robust high flux graphene oxide - nanocellulose membranes for dye removal from water. *J Hazard Mater.* 2019;371(February):484-493. doi:10.1016/j.jhazmat.2019.03.009
127. Jasper EE, Ajibola VO, Onwuka JC. Nonlinear regression analysis of the sorption of crystal violet and methylene blue from aqueous solutions onto an agro-waste derived activated carbon. *Appl Water Sci.* 2020;10(6):1-11. doi:10.1007/s13201-020-01218-y
128. Banerjee S, Chattopadhyaya MC. Adsorption characteristics for the removal of a toxic dye , tartrazine from aqueous solutions by a low cost agricultural by-product. *Arab J Chem.* 2017;10:S1629-S1638.

doi:10.1016/j.arabjc.2013.06.005

129. Silva LE, dos Santos A de A, Torres L, et al. Redispersion and structural change evaluation of dried microfibrillated cellulose. *Carbohydr Polym.* 2021;252(June 2020). doi:10.1016/j.carbpol.2020.117165
130. Nordenström M, Kaldéus T, Erlandsson J, Pettersson T, Malmström E, Wågberg L. Redispersion Strategies for Dried Cellulose Nanofibrils. *ACS Sustain Chem Eng.* 2021;9(33):11003-11010. doi:10.1021/acssuschemeng.1c02122
131. Ballesteros JEM, dos Santos V, Mármol G, Frías M, Fiorelli J. Potential of the hornification treatment on eucalyptus and pine fibers for fiber-cement applications. *Cellulose.* 2017;24(5):2275-2286. doi:10.1007/s10570-017-1253-6
132. Wan JQ, Wang Y, Xiao Q. Effects of hemicellulose removal on cellulose fiber structure and recycling characteristics of eucalyptus pulp. *Bioresour Technol.* 2010;101(12):4577-4583. doi:10.1016/j.biortech.2010.01.026